Characterization of salt hydrates MgCl2.6H2O and MgSO4.7H2O for seasonal sorption heat storage

Scherpenborg, R.A.A.

Award date:
2012

Characterization of salt hydrates $MgCl_2.6H_2O$ and $MgSO_4.7H_2O$ for seasonal sorption heat storage

R.A.A. Scherpenborg

Report number: WET 2013.06

TU/e Master Thesis
June, 2012

Engineering thesis committee:
Prof. dr. ir. H.A. Zondag (TU/e, ECN)
Prof. dr. ir. A.A. van Steenhoven (TU/e)
Prof. dr. P.H.L. Notten (TU/e)
dr. ir. C.C.M. Rindt (TU/e)
dr. S.V. Gaastra-Nedea (TU/e)

Eindhoven University of Technology
Department of Mechanical Engineering
Division Thermo Fluids Engineering
Energy Technology group

Abstract

Magnesiumchloride hexahydrate ($MgCl_2.6H_2O$) and Magnesiumsulfate heptahydrate ($MgSO_4.7H_2O$) are promising salt hydrates for seasonal sorption heat storage due to their high energy density, low cost and non-toxicity. However, these salt hydrates posses some issues that need to be further understood and possibly solved before they can be applied as heat storage media.
The main issue with $MgCl_2.6H_2O$ is the hydrolysis of the material. Hydrolysis reduces the amount of active material and thereby reduces the efficiency and heat storage capacity of the heat storage system. $MgSO_4.7H_2O$ on the other hand, possesses issues with respect to the kinetics of reaction.
The rehydration kinetics of this material is too slow to generate a sufficient temperature rise for the application as a seasonal storage medium.

The hydrolysis of $MgCl_2.6H_2O$ was investigated using a tubular furnace in combination with a water bath and additional pH sensor. It was found that hydrolysis occurs in the whole dehydration range of $MgCl_2.6H_2O$ to $MgCl_2.H_2O$, with the highest hydrolysis rates after dehydration to $MgCl_2.2H_2O$.
A high pressure DSC was used to investigate the kinetics of reaction for the dehydration and rehydration of $MgSO_4.7H_2O$. It was found that the kinetics of reaction can be increased with an increasing water vapor pressure, consistent with the Topley-Smith effect. The lowest reaction rate was found at a p_{H2O} of 8 mbar while the highest reaction rate was achieved at 50 mbar p_{H2O}.
Finally, both salt hydrates were used for dehydration-hydration cycles in a packed bed reactor, which simulates the practical operating conditions of an open sorption heat storage system.
The packed bed reactor, with a volume of 0.65 dm^3, was able to deliver a temperature rise of 15 °C for about 10 hours at a corresponding heating power of 15W during the hydration of $MgCl_2.2H_2O$. A heat release of 1.48 GJ/m^3 was achieved at a reactor inlet temperature of 30°C, 13 mbar p_{H2O} and a massflow rate of 50 L/min. The hydration of $MgSO_4.H_2O$ resulted in a temperature rise of 5°C and 18°C for about 30 minutes at a water vapor pressure of 13 and 50 mbar respectively. The corresponding heat release was equal to 0.013 GJ/m^3 and 0.148 GJ/m^3.

Contents

Nomenclature

A	Frequency factor	[1/s]
c_p	Heat capacity	[J/kg K]
C	Concentration	[mol]
E_a	Activation energy	[J/mol]
$f(\alpha)$	Reaction model equation	[-]
G	Gibbs free energy	[J]
H	Enthalpy	[J/mol]
k	Arrhenius constant	[1/s]
m	Mass	[kg]
$\dot{m}$	Mass flow rate	[kg/s]
n	Amount of moles	[-]
p	Pressure	[Pa]
$\dot{q}$	Power	[W]
R	Gas constant	[J/mol K]
S	Entropy	[J/mol K]
T	Temperature	[K]
UA	Overall heat transfer coefficient	[W/K]
V	Volume	[m^3]

Greek symbols

α	Mass fraction reacted	[-]
β	Heating rate	[K/min]

Subscripts

eq	Equilibrium
r	Reaction
T	Temperature corrected
0	Standard conditions

1 Introduction

Households and offices are responsible for about 30% of the total energy demand in the Netherlands [1]. About 65% of this energy demand consists of space heating and water heating [2]. In order to reduce the need for fossil fuels, offices and households can use solar energy to meet their heating demand.
The downside of using solar energy for heating purposes is that there is a mismatch between solar energy production and the heating demand, as can be seen from Figure 1 [3]. In summer there is an excess of solar energy while there is an excess of energy consumption in winter. Energy storage is therefore needed to overcome the difference in energy demand and energy supply.

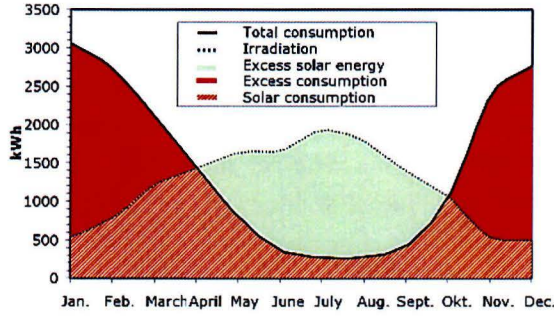

Figure 1: Seasonal energy demand and supply in the Netherlands [3]

There are multiple ways to store heat. The most conventional method is sensible heat storage, by which heat is stored most often in water using for instance a solar boiler. However, seasonal heat storage in water would require a tank of about 40 m^3, based on a winter heating demand of 6 GJ for a passive house, which is too large to be placed in an average household [4].
An alternative is storing heat by using phase change materials (PCM). Large amounts of heat are absorbed by melting of a certain material, without change in temperature. This latent heat storage has an energy density which is about 2 to 5 times larger in comparison to sensible heat storage.
The highest energy density however, is obtained using thermochemical materials (TCM) such as salt hydrates, which have a 5 to 10 times higher energy density than water (1 GJ/m^3 for a packed bed) [4]. The implementation of TCM for seasonal heat storage would require a storage of about 6 m^3 to meet the winter heating demand.

Magnesiumchloride hexahydrate ($MgCl_2.6H_2O$) and Magnesiumsulfate heptahydrate ($MgSO_4.7H_2O$) are promising salt hydrates for seasonal sorption heat storage due to their high energy density, low cost and non-toxicity [5]. However, these salt hydrates posses some issues that need to be further understood and possibly solved before they can be applied as heat storage media.
The main issue with $MgCl_2.6H_2O$ is the hydrolysis of the material. Hydrolysis reduces the amount of active material and thereby reduces the efficiency and heat storage capacity of the heat storage system. $MgSO_4.7H_2O$ on the other hand, possesses issues with respect to the kinetics of reaction.

The rehydration kinetics of this material are too slow to generate a sufficient temperature rise for the application as a seasonal storage medium.
The main focus of this research will be on the characterization of the issues described above. These characterizations will all be performed within the scope of seasonal solar heat storage.

The hydrolysis of $MgCl_2.6H_2O$ will be analyzed by means of a tubular furnace. This furnace supplies the heat required for dehydration and hydrolysis of the material. The HCl that is released during hydrolysis is captured in a water bath, so that a quantification of the amount of hydrolysis is possible. The sample size in the reactor is relatively large, ~ 10 gram, which makes it possible to take samples during the experiment for additional XRD and SEM-EDAX measurements. The quantification of the hydrolysis will be performed at different sample thicknesses, different furnace temperatures and different mass flows through the reactor.
The kinetics of reaction of $MgSO_4.7H_2O$ are analyzed with a differential scanning calorimeter (DSC). With a DSC it is possible to accurately determine the heat released or absorbed during (de)hydration of $MgSO_4.7H_2O$ which enables an accurate analysis of the kinetics of reaction. These reaction kinetics are characterized for different water vapor pressures.
Finally, a laboratory scale packed bed reactor is used to study the application of both $MgCl_2.6H_2O$ and $MgSO_4.7H_2O$ as a heat storage medium. The heat release and heat absorbed will hereto be analyzed for different inlet temperatures and different mass flows though the reactor for the (de)hydration of $MgCl_2.6H_2O$ and for different water vapor pressures for the (de)hydration of $MgSO_4.7H_2O$.

A literature background on seasonal heat storage will be given in chapter 2, together with a literature study of both $MgCl_2.6H_2O$ and $MgSO_4.7H_2O$. Next, the theoretical fundamentals of thermodynamics and kinetics of reaction used for the characterization of both salt hydrates will be described in chapter 3. In chapter 4, the different experimental setups and methods will be discussed. Finally, the results and discussion will be presented in chapter 5.

2 Literature Background

2.1 Seasonal Solar Thermochemical Heat Storage

Thermochemical heat storage is characterized by separating the storage material into multiple components using heat. By bringing these components together, sorption occurs and heat is released again. Heat is stored in TCM's according to the following reversible chemical reaction:

$$A + B = C + heat \tag{1}$$

Heat is stored in TCM's by means of two possible processes, namely by physical adsorption (physisorption) and chemical absorption (chemisorption). Physical adsorption is a surface reaction in which a gas (sorbate) binds to the surface of a solid material (sorbent), which does not affect the structure of the sorbent. For chemical absorption, the sorption takes place on a molecular level, affecting both the composition and the morphology of the sorbent.

Heat is stored in salt hydrates by means of chemical absorption according to the following reaction:

$$Salt.nH_2O\ (s) + heat \leftrightarrow Salt(s) + nH_2O(g) \tag{2}$$

Equation 2 states that heat is stored by dehydration of the hydrated salt ($salt.nH_2O$). This results in a (partially) dehydrated salt and water vapor (nH_2O). The stored heat can be released again when water vapor is added to the salt. Equation 2 also implies that the heat can be stored for a very long time without energy losses, as long as the salt and the water vapor are separated, which is a great advantage over sensible heat storage and latent heat storage.

Another important advantage of using salt hydrates as a storage medium is that these salts can be dehydrated and rehydrated under the practical operating conditions of seasonal solar heat storage.
A schematic overview of a thermochemical open sorption heat storage system is given in Figure 2 [4]. The storage is charged during summer by the heat produced by the solar array. A fan is used to drive the heated air through the packed bed which dehydrates (charges) the hydrated salt. When this stored heat is needed again, cold and moist air is driven through the reactor, which results in rehydration of the salt.

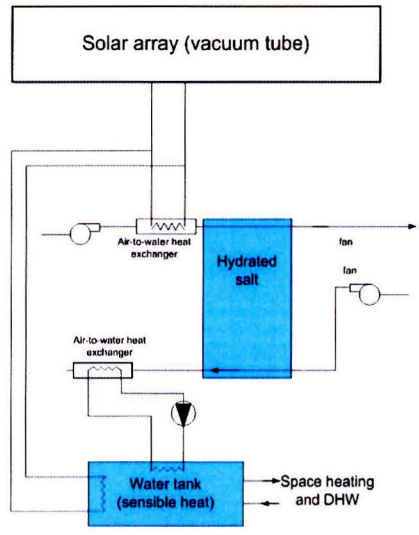

Figure 2: Schematic overview of thermochemical open sorption heat storage system [4]

The solar array is heated in summer up to a operating temperature of 150°C. The ambient water vapor pressure (p_{H2O}) in the summer varies between 8 to 20 mbar with an average of 13 mbar in the Dutch climate. The p_{H2O} in the winter however varies between 5 to 10 mbar. In order to increase the water vapor pressure needed for the rehydration reaction in the winter, a borehole is used at 10°C. The water vapor pressure generated at 10°C is equal to 13 mbar, which is the reference vapor pressure used for open seasonal storage systems.

2.2 Thermochemical Materials

Various researches [3,6,7,8,9,10] have shown promising results for $MgSO_4.7H_2O$ and $MgCl_2.6H_2O$ for the application as TCM for seasonal sorption heat storage. A summary of the literature study of the dehydration and rehydration characteristics of these salt hydrates will be given in this chapter.

2.2.1 $MgCl_2.6H_2O$

The dehydration of $MgCl_2.6H_2O$ was investigated by Ferchaud et al. under 12 mbar of water vapor pressure [5]. The results are shown in the following figure:

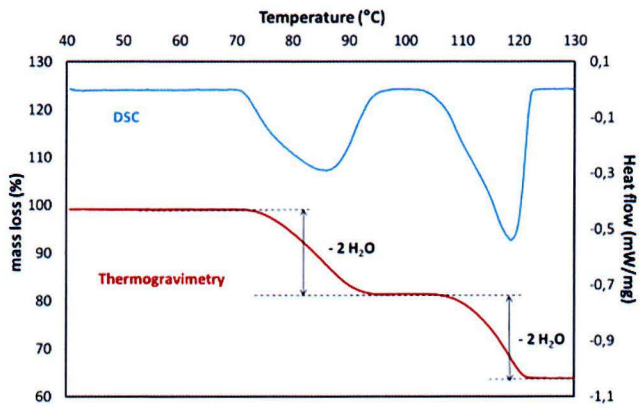

Figure 3: DSC- and Thermogravimetry signal for the dehydration of $MgCl_2.6H_2O$ at 12 mbar p_{H2O} with β = 0,5°C/min [5]

Figure 3 clearly shows two dehydration steps. The first dehydration step occurs at an onset temperature of 70°C in which $MgCl_2.6H_2O$ is dehydrated to $MgCl_2.4H_2O$. The second dehydration step starts at an onset temperature of 105°C and dehydrated the $MgCl_2.4H_2O$ further to $MgCl_2.2H_2O$. This mass loss can also be seen from the two endothermic peaks in the DSC signal, corresponding to the formation of a lower hydrated phase. The fully hydrated $MgCl_2.6H_2O$ thus looses two water molecules in two consecutive steps up to a sample temperature of 130°C.

Increasing the sample temperature further results in the formation of MgClOH and HCl as can be seen from the XRD results shown in Figure 4 [5]. This hydrolysis of the salt hydrate is a result of the following side reaction: $MgCl_2.2H_2O(s) \rightarrow MgClOH(s) + HCl(g) + H_2O$. This reaction reduces the amount of active material and thereby reduces the amount of heat that can be stored in the material. The formation of HCl is also undesirable because the gas is corrosive to the system. Based on these results, the dehydration temperature should be limited to 130°C.

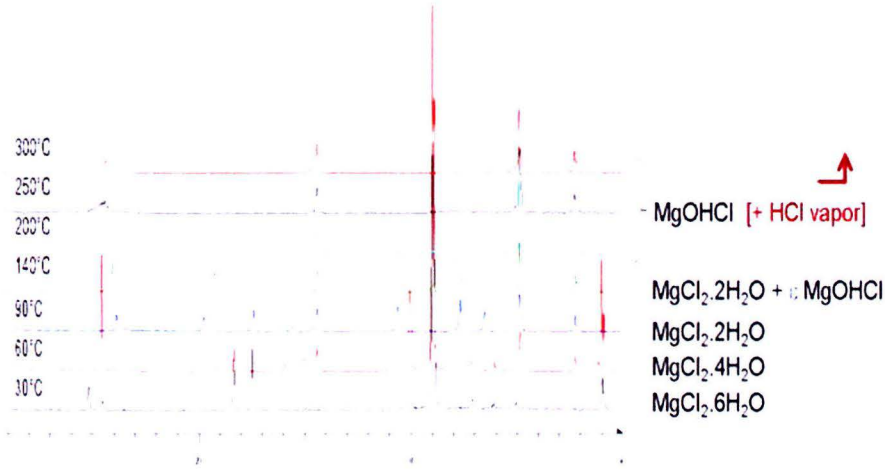

Figure 4: XRD spectra for the dehydration of $MgCl_2.6H_2O$ at 12 mbar p_{H2O} [5]

Research done by Kipourous et al. has shown that the hydrolysis of $MgCl_2.6H_2O$ depends on the HCl vapor pressure (p_{HCl}), as can be seen from the equilibrium lines of $MgCl_2$ shown in Figure 5 [11].

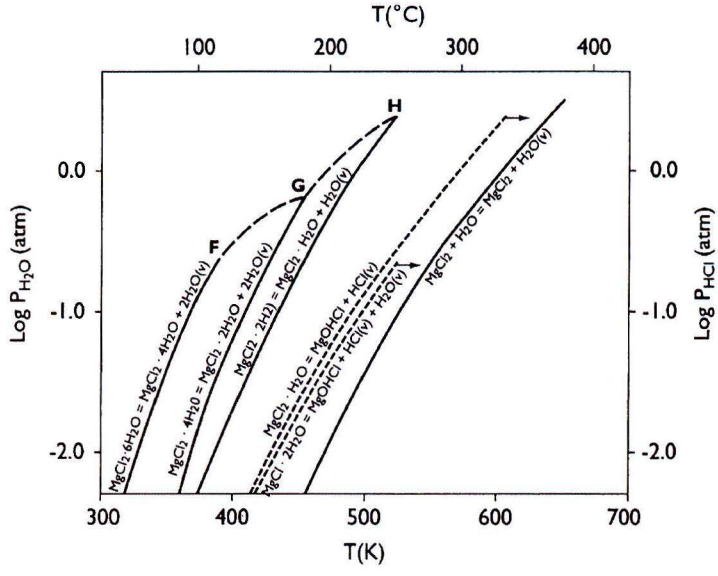

Figure 5: Equilibrium curves for the dehydration reactions and hydrolysis of $MgCl_2.6H_2O$ [11]

The equilibrium lines shown in Figure 5 represent the exact equilibrium states for certain reactions, given for the H_2O and HCl vapor pressure as a function of the temperature. The figure shows four dehydration equilibrium lines as a function of p_{H2O} and two decomposition equilibrium lines as a function of p_{HCl}. The hydrolysis reactions start at around 430 K (157°C) for a p_{HCl} equal to 10^{-2} atm. These reactions start at even lower temperatures when the p_{HCl} is lower. This corresponds with the

results from Ferchaud et al. [5], in which the decomposition reaction occurred at a sample temperature of above 130°C.

In addition to dehydration, the rehydration of $MgCl_2$ must be sufficiently fast and at sufficiently high temperature in order to realize a significant temperature rise and heating power. Figure 6 shows the dehydration-rehydration cycle of $MgCl_2$ at 13 mbar water vapor pressure [12].

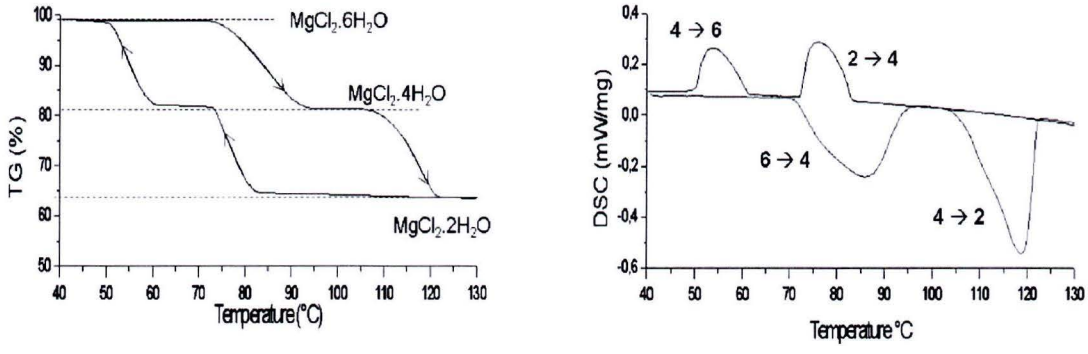

Figure 6: Thermogravimetry signal (left) and DSC signal (right) of the dehydration-rehydration cycle of $MgCl_2.6H_2O$ at 13 mbar p_{H2O} with β = 0,5°C/min (during dehydration) and 0,2°C/min (during hydration) [12]

These results correspond to the results shown in Figure 3 and Figure 4. The dehydration of $MgCl_2.6H_2O$ takes place in two consecutive reactions, each releasing two water molecules. These water molecules are taken up again upon rehydration, represented by the two exothermic peaks in the DSC signal and the mass gain in the TG signal. Figure 6 also clearly shows a hysteresis which implies that the heating rate is relatively fast with respect to the kinetics of reaction. A crystal energy density of 1.4 GJ/m^3 was found from these DSC results for the rehydration of $MgCl_2.2H_2O$ to $MgCl_2.6H_2O$, which corresponds to 0.7 GJ/m^3 for a packed bed with 50% porosity [5].

The high heat release upon rehydration is a result of the fast water vapor uptake due to the high hygroscopic character of $MgCl_2$. This high hygroscopic character can lead to overhydration of the salt hydrate. Overhydration implies that the salt hydrate takes up water to such an extent that it starts to dissolve in its own solution. This results in a gel-like solution that forms an impervious layer when the sample is dehydrated again. The impervious layer reduces the water vapor transport through the bed and therefore reduces the water vapor uptake of the material. Figure 7 shows the phase diagram for $MgCl_2.6H_2O$ for the water vapor pressure as a function of the sample temperature [13]. From this figure it can be seen that a minimum temperature of 30°C is required to prevent melting (or overhydration) at a p_{H2O} of 13 mbar, which implies that the material is highly unstable under atmospheric conditions.

At ECN, a prototype lab scale open sorption heat storage system was built and tested, with 20 liters of $MgCl_2.6H_2O$ as a heat storage material [4]. The high heat release during hydration resulted in a temperature rise of about 15°C in the bed, heating the air from 50°C to 65°C. Incoming moist air at 10°C was preheated to 50°C by the outgoing dried air through an air-to-air heat exchanger [4]. The prototype storage was found to be able to deliver heat at 60°C for about 20 hours, with an air flow equal to 500 liter/min, corresponding to a heating power of 50 W.

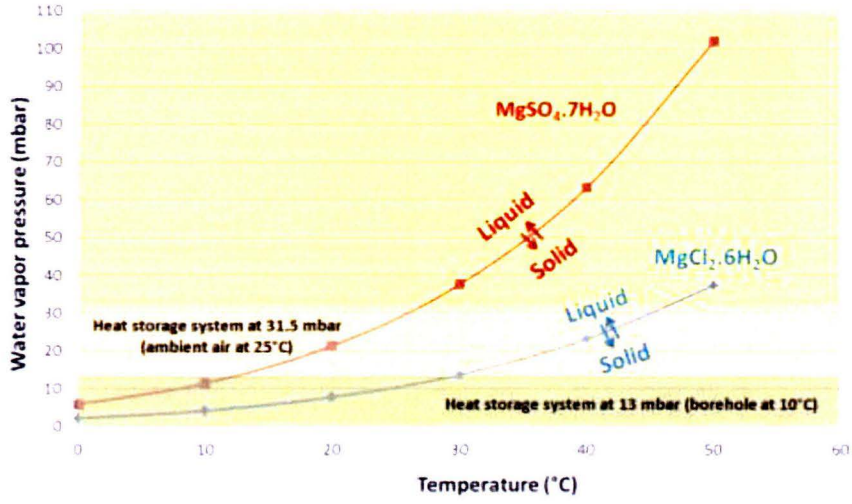

Figure 7: Phase diagram of $MgCl_2$.6H2O for the water vapor pressure as function of the sample temperature [13]

2.2.2 $MgSO_4.7H_2O$

Figure 8 shows the results of XRD measurements of the dehydration and rehydration reactions of $MgSO_4.7H_2O$ under a water vapor pressure of 13 mbar [12]. The dehydration takes place in two consecutive steps. In the first step, the fully hydrated $MgSO_4.7H_2O$ is dehydrated to $MgSO_4.6H_2O$ at a sample temperature between 30°C and 40°C, in which the sample retains a crystalline structure. In the second step, the crystalline $MgSO_4.6H_2O$ is reformed to an amorphous phase at a sample temperature between 60°C and 80°C. This amorphous phase is characterized by a featureless signal in the XRD spectrum. The formation of the amorphous phase during dehydration of $MgSO_4.7H_2O$ may be related to a slow reaction rate at a water vapor pressure of 13 mbar [14].
During rehydration, the material starts to recrystallize within 30 minutes at 25°C [12], which results in the formation of $MgSO_4.6H_2O$. Figure 8 also shows that the material is not further rehydrated to $MgSO_4.7H_2O$, which is in agreement with research done by Chipera et al. [15]. They stated that the formation of $MgSO_4.7H_2O$ can only be realized at a water vapor pressure above 60 mbar. This implies that full rehydration of $MgSO_4.7H_2O$ cannot be realized in seasonal sorption heat storage, in which the operating water vapor pressure is equal to 13 mbar.

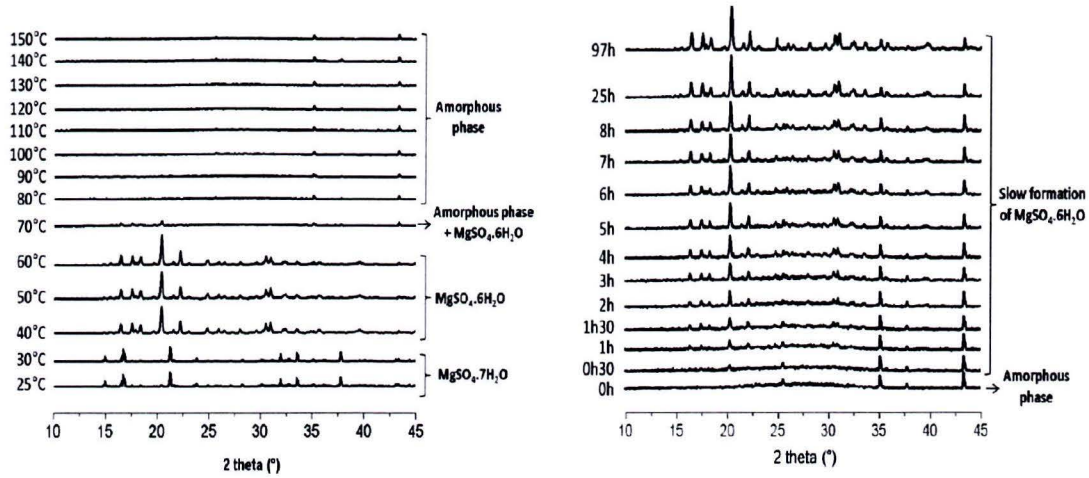

Figure 8: XRD spectrum of the dehydration performed at a heating rate of 1°C/min (left) and rehydration performed at 25°C (right) of $MgSO_4.7H_2O$ [12]

Figure 9 shows the results of thermal analysis measurements for the dehydration/rehydration cycle of $MgSO_4.7H_2O$ at 13 mbar water vapor pressure, done by Ferchaud et al. [12]. These results correspond with the abovementioned XRD measurement results.

The two consecutive dehydration steps can be clearly distinguished by the two endothermic peaks in the DSC signal and the mass loss in the Thermogravimetry (TG) signal. From the TG measurement, it can also be seen that the mass of the amorphous phase at 150°C is equal to the mass of $MgSO_4.H_2O$. This implies that in the second dehydration step, $MgSO_4.6H_2O$ is dehydrated to $MgSO_4.H_2O$, by releasing five water molecules.

Hydration of the $MgSO_4.H_2O$ starts at a sample temperature below 30°C. After 90 hours, the material is fully hydrated to $MgSO_4.6H_2O$, but the hydration heat release is only observed during the first ten hours of hydration. This implies that after these first ten hours, the water vapor uptake is too low to produce a significant heating power.

This low water vapor uptake results also in a low overhydration temperature, as can be seen from Figure 7 in the previous paragraph. The minimum required temperature to prevent overhydration of $MgSO_4.7H_2O$ is 12°C at a water vapor pressure of 13 mbar, which is much lower than the overhydration temperature for $MgCl_2.6H_2O$.

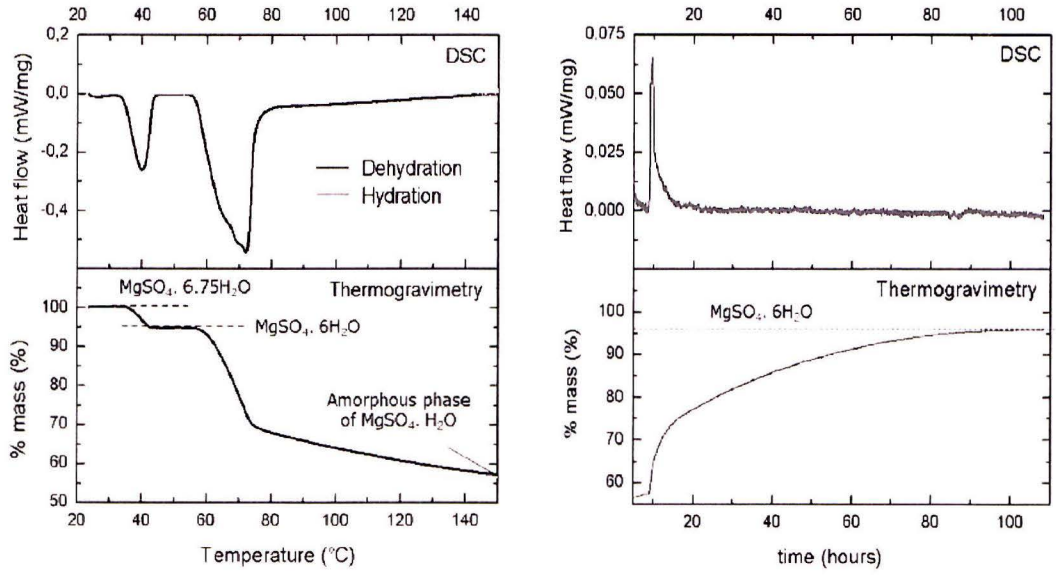

Figure 9: DSC and Thermogravimetry signal of the dehydration and rehydration of $MgSO_4.7H_2O$ at 13 mbar p_{H2O} as a function of the sample temperature at β = 0,5°C/min (left) and time, isothermal at 25°C (right) [12]

A possible way to improve the kinetics of reaction is by changing the water vapor pressure. Topley and Smith found a relation between the water vapor pressure and the reaction rate in their research on the dehydration of $MnC_2O_4.2H_2O$ [16]. A decreasing trend in the reaction rate, for an increasing water vapor pressure, would be expected based on basic thermodynamics. Topley and Smith found however that after a certain water vapor pressure (the critical water vapor pressure), the reaction rate increases again up to a maximum, after which the reaction rate decreases with increasing p_{H2O}, as can be seen from Figure 10. This increase in the reaction rate has been attributed to the additional formation of cracks and channels as a result of the increased water vapor pressure, which facilitate the water vapor removal [17]. This trend has been found for several crystalline hydrates and has been established in literature as the Topley-Smith effect.

The lowest dehydration reaction rates for $MgSO_4.7H_2O$ were obtained at a p_{H2O} of around 8 mbar, while the highest rates were found for a p_{H2O} of around 50 mbar [18,19,20]. From Figure 10 it can be seen that the reaction rate at 13 mbar is very close to the minimal reaction rate at the critical p_{H2O} of 8 mbar. This indicates that under the practical operating conditions of seasonal heat storage, the dehydration of $MgSO_4.7H_2O$ will always proceed with a slow reaction rate and a slow reorganization of the lattice structure. When the formation of the amorphous phase is related to the slow reaction rate during dehydration, it may imply that the formation of the amorphous phase can be prevented by increasing the reaction rate according to the Topley-Smith effect.

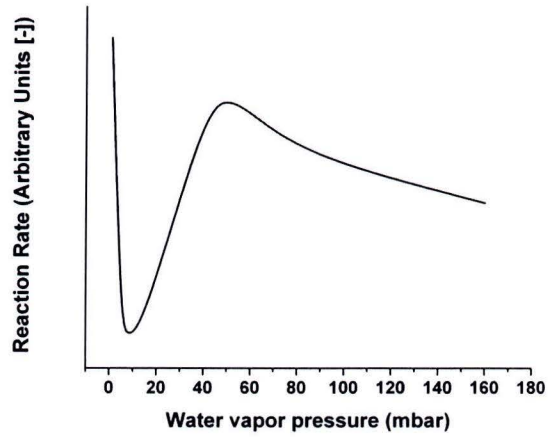

Figure 10: Topley-Smith effect for the dehydration of $MgSO_4.7H_2O$ based on data from literature [18,19,20]

Van Essen et al. have realized a temperature increase of 6°C during rehydration of $MgSO_4.H_2O$ [7] in a closed sorption reactor. These experimental results were obtained at a reactor temperature of 25°C and a water vapor pressure equal to 32 mbar (generated by an evaporator at 25°C). At 13 mbar p_{H2O}, the temperature increase in the reactor was only 4°C. In an open sorption system however, the air flowing through the reactor also needs to be heated, indicating that the temperature rise in such a system will be even lower than mentioned above.

3. Theory

3.1 Thermodynamics

Thermodynamics are used to determine the equilibrium pressure, equilibrium temperature and enthalpy of reaction for the dehydration and rehydration reactions of the salt hydrates.
The equilibrium curves can be calculated from the values of the enthalpy change and entropy change occurring in a reaction. The direction of a reaction is determined by the change in the Gibbs free energy. When this change is negative, the reaction is spontaneous. When the change is positive, the reaction is non-spontaneous. If the change is in the Gibbs free energy is equal to zero, the reaction is in equilibrium.
The change in Gibbs energy under standard conditions is calculated using the following equation, (vapor pressure = 1 bar):

$$\Delta G = \Delta G_0 = \Delta H_0 - T\Delta S_0 \tag{3}$$

With ΔG being the change in free Gibbs energy, ΔG_0 the change in Gibbs free energy under standard conditions, ΔH_0 the change in enthalpy under standard conditions, ΔS_0 the change in entropy under standard conditions and T the temperature in Kelvin.

ΔH_0 and ΔS_0 of a reaction are calculated from the difference in enthalpy of formation and entropy between the reaction products and reactants.
As can be seen from Figure 11, ΔH_0 represents the difference in energy level of reactant (X) and reaction product (Y). When $\Delta H_0 > 0$, the reaction is endothermic which means that the reaction requires heat. When $\Delta H_0 < 0$, the reaction is exothermic which implies that heat is released during the reaction.
The activation energy, E_a, represents the energy barrier that must be overcome to permit the transformation of reactants into products.

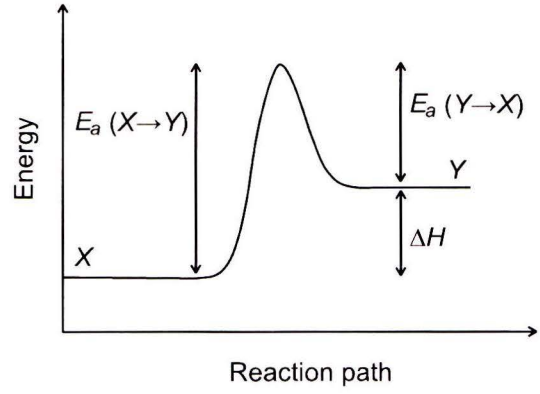

Figure 11: Reaction energy level versus reaction path

If a reaction occurs under non-standard conditions (vapor pressure ≠ 1 bar), equation 3 has to be extended:

$$\Delta G = \Delta G_0 + RTlnQ \tag{4}$$

With R being the universal gas constant.

Q is calculated in the following way:

$$Q = \frac{C_{product1} \cdot C_{product2}}{C_{reactant1} \cdot C_{reactant2}} = \frac{p_{product1} \cdot p_{product2}}{p_{reactant1} \cdot p_{reactant2}} \tag{5}$$

With *C* being the concentration and *p* the pressure in bar.

For the calculation of the equilibrium temperature, only the concentration of reactants and products in the gaseous phase need to be taken into account. In the case of de dehydration/rehydration reactions of salt hydrates this term will be equal to ${p_{H2O}}^n$ or $\frac{1}{{p_{H2O}}^n}$ for dehydration and rehydration respectively, with *n* being the number of water vapor molecules in the reaction equation.
The equilibrium temperature and equilibrium pressure can be calculated by rewriting equation 4 ($\Delta G = 0$):

$$T_{eq} = \frac{\Delta H_0}{\Delta S_0 - Rln(p_{H2O}^n)} \tag{6}$$

$$p_{H2O,eq}^n = exp\left(\frac{-\Delta H_0 + T\Delta S_0}{RT}\right) \tag{7}$$

A temperature correction has to be applied for the calculation of ΔH and ΔS at high temperatures. The heat of evaporation reduces with increasing temperature until the difference between the liquid and the gas phase disappears and the evaporation energy becomes equal to zero. In addition, the entropy of evaporation decreases with increasing temperature. The corrected values for ΔH and ΔS can be calculated by the following equations:

$$\Delta H_T = \Delta H_o + \Delta C_p(T - 298) \tag{8}$$

$$\Delta S_T = \Delta S_0 + \Delta C_p ln\left(\frac{T}{298}\right) \tag{9}$$

With ΔC_p being the difference in heat capacity between products and reactants.

Based on the equations described above, the following equilibrium curves can be calculated for the dehydration/rehydration and hydrolysis of $MgCl_2.6H_2O$:

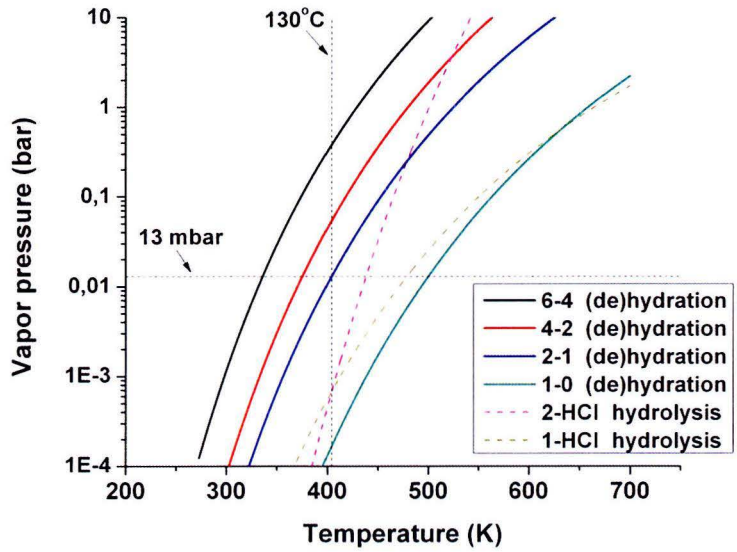

Figure 12: Equilibrium curves for the (de)hydration and hydrolysis of $MgCl_2.6H_2O$ with the solid- and dashed curves depending on the p_{H2O} and p_{HCl} respectively

Figure 12 shows the equilibrium curves of $MgCl_2.6H_2O$ for the vapor pressure as a function of the temperature, based on the values for ΔH_0 and ΔS_0 as shown in table 1. The temperature correction, as described by equations 8 and 9, has been applied for these curves. For the (de)hydration, the equilibrium curves are depending on the water vapor pressure (p_{H2O}) while the hydrolysis depends on the HCl vapor pressure (p_{HCl}). The hydrolysis reaction, $MgCl_2.2H_2O \rightarrow MgClOH + HCl + H_2O$, depends on both p_{H2O} and p_{HCl}. For this equilibrium curve (2-HCl), it was assumed that the water vapor pressure was equal to 13 mbar.

From Figure 12 it can be seen that the 2-1 (de)hydration is exactly in equilibrium at 13 mbar p_{H2O} and 130°C. At these conditions, it can also be seen that the hydrolysis reactions are thermodynamically favored over the 2-1 dehydration at a p_{HCl} lower than 1 mbar.

	ΔH_0 (KJ/mol)	ΔS_0 (J/mol.K)	C_p (J/mol.K)	M
$MgCl_2.6H_2O$	**-2499.02**	**366.1**	**315.06**	**203.30268**
$MgCl_2.4H_2O$	-1898.99	264	241.42	167.27212
$MgCl_2.2H_2O$	**-1279.72**	**179.9**	**159.2**	**131.24156**
$MgCl_2.H_2O$	-966.63	137.2	115.27	113.22628
$MgCl_2$	**-640.91**	**89.62**	**71.38**	**95.211**
MgClOH	-799.6	83.7	70.83	76.76534
$MgSO_4.7H_2O$	-3388.71	372		246.47456
$MgSO_4.6H_2O$	**-3087.0**	**348.1**		**228.45928**
$MgSO_4.H_2O$	-1602.1	126.4		138.38288
HCl	-92.13	186.91	29.12	36.46094
H_2O (g)	**-241.83**	**188.84**	**33.58**	**18.01528**

Table 1: Properties of selected salt hydrates [21]

3.2 Kinetics of Reaction

The reaction kinetics describe the speed at which a certain reaction reaches its equilibrium state. In this chapter, a few kinetic parameters will be discussed, which will be used for kinetic analysis in chapter 5.

The kinetics of reaction are analyzed by means of the reaction rate $\frac{d\alpha}{dt}$, which is the derivative of the reacted mass fraction, α, with respect to time. The reaction rate can be calculated using the following equation:

$$\frac{d\alpha}{dt} = f(\alpha).k \tag{10}$$

With *k* being the Arrhenius constant defined as:

$$k = A.exp\left(\frac{-E_a}{RT}\right) \tag{11}$$

With *A* being the pre-exponential factor, E_a the activation energy, *R* the universal gas constant and *T* the temperature. $f(\alpha)$ in equation 10 is the reaction model equation, a certain function of α depending on the type of reaction.

The reaction rate can also be defined as the derivative of α with respect to the temperature, by which equation 10 is rewritten in the following way, :

$$\frac{d\alpha}{dT} = \frac{d\alpha}{dt}\cdot\frac{dt}{dT} = \frac{1}{\beta}f(\alpha).k \tag{12}$$

In which β (also defined as $\frac{dT}{dt}$) is the heating rate.

The reacted mass fraction at time i is defined in the following way:

$$\alpha_i = \frac{m_0 - m_i}{m_0 - m_f} \tag{13}$$

With m_0 being the initial mass of the sample, m_i the mass of the sample at time i and m_f the final sample mass. This parameter is a measure for the amount of material that has reacted.

The value for the activation energy can be calculated by various methods. The method applied by Ruiz et al. [22] is the non-integrated Flynn, Wall and Ozawa (FWO) method. This method is based on the following equation, which is obtained by rewriting equation 11 and 12:

$$\ln(\beta) = ln\left(A\frac{f(\alpha)}{d\alpha/dT}\right) - \frac{E_a}{RT_\alpha} \tag{14}$$

The method involves measuring the temperatures corresponding to fixed values of α from experiments performed at different heating rates, β, as shown in Figure 13 (for α = 0.5). By plotting

$\ln(\beta)$ against $\frac{1}{T_\alpha}$, the activation energy can be determined from the slope of the curve, which is equal to $-\frac{E_\alpha}{R}$. For this method it is thus necessary that the reactions proceed in a consistent order according to the used heating rate. The reaction at 1°C/min must proceed before the reaction at 2°C/min and so on in order to obtain a straight line in the $\ln(\beta)$ vs. $\frac{1}{T_\alpha}$ plot.

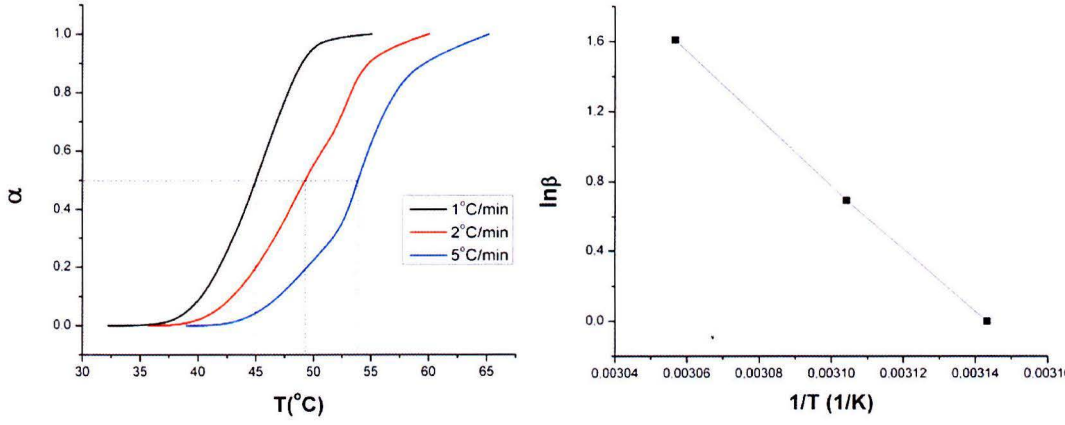

Figure 13: Mass fraction reacted as a function of temperature for different heating rates (left) and natural logarithm of the heating rate versus 1/temperature for fixed values of α (right)

The pre-exponential factor can be determined according to the so called compensation effect [22,23]. This correlation between the activation energy and the pre-exponential faction is defined in the following equation [22,23]:

$$\ln(A) = a.E_A + b \tag{15}$$

Where *a* and *b* are constants. Ruiz et al. [22] have found the following values for the parameters *a* and *b* for the dehydration of $MgSO_4.7H_2O$ in a nitrogen atmosphere:

	β = 1K/min	β = 2K/min	β = 5K/min
a x 10^4 (mol/J)	3.4	3.2	3.2
b	-0.3865	-0.3445	-0.3275

Table 2: Value of the parameters a and b in the compensation effect for the dehydration of $MgSO_4.7H_2O$ in a nitrogen atmosphere for different heating rates

Using the FWO-method and the compensation effect, Ruiz et al. have found values for the activation energy and the pre-exponential factor for the dehydration of $MgSO_4.7H_2O$, as shown in Figure 14. In these graphs, α = 0 corresponds to $MgSO_4.7H_2O$ and α = 1 to $MgSO_4.H_2O$. These data will be used as reference data for the characterization of $MgSO_4.7H_2O$ in chapter 5.2.

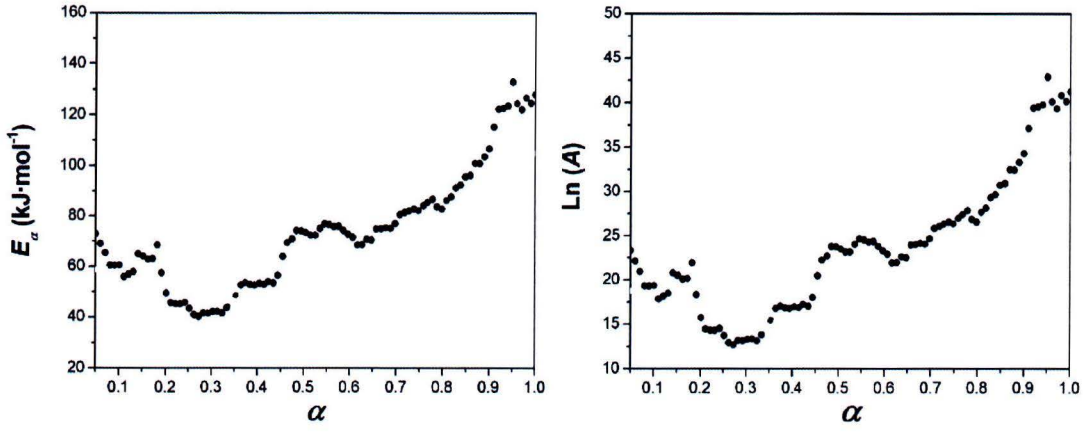

Figure 14: Values for the activation energy (left) and pre-exponential factor (right) for the dehydration of $MgSO_4.7H_2O$ obtained by Ruiz et al. [22]

The reaction model equation, as introduced above in equation 10, depends on the dominant process, or a combination of processes in a certain reaction. Solid state reactions are controlled by three main processes: nucleation, interface advance (growth) and diffusion [24]. The most important reaction models used in kinetic analysis of solid state reactions are shown in the following figure:

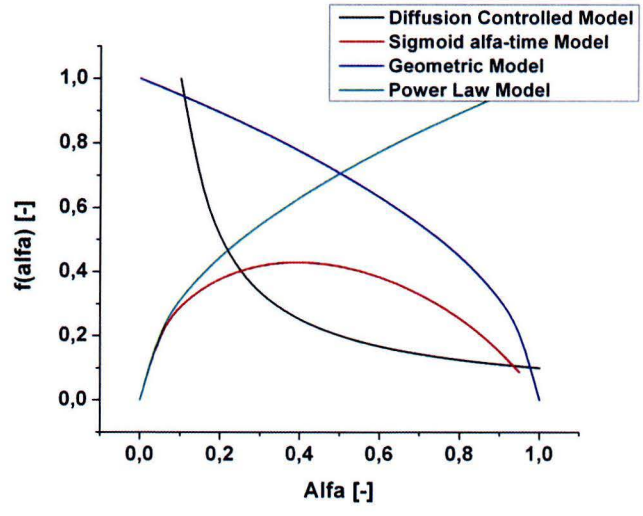

Figure 15: Overview of the most important reaction models used in kinetic analysis of solid state reactions [25]

The sigmoid α-time model is based on an infrequently occurring nucleation, implying that nucleation is the rate-determining step.

The geometrical model is based on the initial rapid (instantaneous) nucleation across all crystal faces. The hereby formed reaction interfaces advance at a constant rate in the absence of diffusion effects.

In the power law model, the instantaneous formation of nuclei is assumed in addition to an unrestricted and constant rate of interface growth at all surfaces of these nuclei. The power law

model is only applicable to the early stages of reaction when the assumption of unrestricted nucleus growth is acceptable.

For the diffusion controlled model it is assumed that the diffusion rate of participants to or from an reaction interface is of dominant influence on the reaction rate. The kinetics of dehydration of some crystalline hydrates have been shown to be controlled by the rate of diffusion of water [26].

3.3 Calculation of Kinetics Parameters

3.3.1 Mass Fraction Reacted and Reaction Rate

The mass fraction reacted, as described in chapter 3.2, can be calculated from the DSC signal, which gives the heat flow as a function of time. Integration of this signal gives information about the amount of energy absorbed or released by the material. The mass fraction reacted at time i is then calculated according to the following equation:

$$\alpha_i = \frac{\int_0^i (heat\ flow)dt}{\int_0^\infty (heat\ flow)dt} \tag{16}$$

The denominator is equal to the total energy absorbed or released, whereas the numerator equals the energy absorbed or released during a certain period up to time i. The fraction of these values gives then the value for α. This method gives information about the mass fraction reacted as function of time, from which the reaction rate, $\frac{d\alpha}{dt}$, can be calculated.

3.3.2 Activation Energy

The activation energy, E_a, can be calculated using the Flynn, Wall and Ozawa (FWO) method as described in chapter 3.2. Hereto, DSC measurements are needed which are performed at different heating rates, for instance at 1°C/min, 2°C/min and 5°C/min. Then, the temperatures of these different measurements are compared for fixed values of α. This implies that a set of temperatures is obtained for different values of α. By plotting the natural logarithm of the heating rate, $ln\beta$, versus 1/T, a straight line is obtained, as shown in Figure 13. The slope of this line is equal to $-E_a/R$, with R being the universal gas constant, from which the activation energy can be calculated. This acquired value for E_a corresponds then to a certain predefined value of α. This process can be repeated for different values of α in order to get a trend for the activation energy for a certain reaction.

3.4 Reactor Energy Balances

The general energy balance for an open sorption reactor during dehydration is given by the following equation:

$$\dot{q}_{in} = \dot{q}_{stored} + \dot{q}_{loss} + \dot{q}_{out} \tag{17}$$

In which $\dot{q}_{in}$ is the heat supplied to the reactor by the incoming air, $\dot{q}_{stored}$ is the heat stored in the salt hydrate, $\dot{q}_{loss}$ is the heat loss by heat transfer from the reactor walls to the ambient and $\dot{q}_{out}$ is the heat of the outgoing air.
Equation 17 can be rewritten in the following form:

$$\dot{m}_{air} c_{p,air} (T_{inlet} - T_{outlet}) = m_{salt} c_{p,salt} \frac{dT_{salt}}{dt} + \dot{m}_{vapor} \Delta H_r + UA(T_{salt} - T_{ambient}) \tag{18}$$

In which $\dot{m}_{air}$ is the massflow rate of the air, $c_{p,air}$ is the heat capacity of the air, T_{inlet} is the temperature of the incoming air, T_{outlet} is the temperature of the outgoing air, m_{salt} is the mass of the salt hydrate, $c_{p,salt}$ is the heat capacity of the salt hydrate, $\dot{m}_{vapor}$ is the massflow rate of the water vapor, ΔH_r is the reaction enthalpy, UA is the overall heat transfer coefficient and $T_{ambient}$ is the temperature of the ambient air.

The energy balance for an open sorption reactor during hydration is given by:

$$\dot{q}_{in} + \dot{q}_{hydration} = \dot{q}_{loss} + \dot{q}_{out} \tag{19}$$

In which $\dot{q}_{hydration}$ is the heat release of the salt hydrate during hydration. In this equation, it is assumed that the sensible heat stored in the system is negligible. Equation 19 can be rewritten in the following form:

$$\dot{m}_{vapor} \Delta H_r = UA(T_{salt} - T_{ambient}) + \dot{m}_{air} c_{p,air} (T_{outlet} - T_{inlet}) \tag{20}$$

In which $\dot{m}_{air} c_{p,air} (T_{outlet} - T_{inlet})$ is the heating power of the reactor. In equation 20 it is assumed that all the water vapor in the air flow is absorbed during the hydration of the salt hydrate.

For the calculation of the amount of water present in the air mass flow, the following equation is used:

$$pV = nRT \tag{21}$$

In which p is the pressure, V is the volume, n is the amount of moles and R is the universal gas constant.

4 Experimental Setup and Method

Three experimental setups were used for the characterization of $MgCl_2.6H_2O$ and $MgSO_4.7H_2O$. A tubular furnace is used to analyze the hydrolysis of $MgCl_2.6H_2O$. The kinetics of reaction of $MgSO_4.7H_2O$ will be analyzed by means of a HPDSC. Finally, the application of $MgCl_2.6H_2O$ and $MgSO_4.7H_2O$ as heat storage media will be analyzed in a laboratory scale packed bed reactor. The experimental setup and method of these characterization techniques are described in this chapter.

4.1 Characterization of $MgCl_2.6H_2O$: Tubular Furnace

In order to analyze the dehydration and hydrolysis reactions of $MgCl_2.6H_2O$, an experimental setup is used which consists of three main components: a humidification system, the tubular furnace and a water bath. The main function of this tubular furnace is to heat up the sample of $MgCl_2.6H_2O$, delivering the heat required for the dehydration. The humidification system is used to humidify the incoming air and thereby increase the water vapor pressure before the air enters the furnace. The water bath, which is located right after the exit of the tubular furnace, is used to capture the HCl, which is possibly formed during the dehydration of the $MgCl_2.6H_2O$.
The material sample of about 10 gram is contained in a crucible over which the air flow is driven. Figure 16 shows the schematic overview of the system setup.

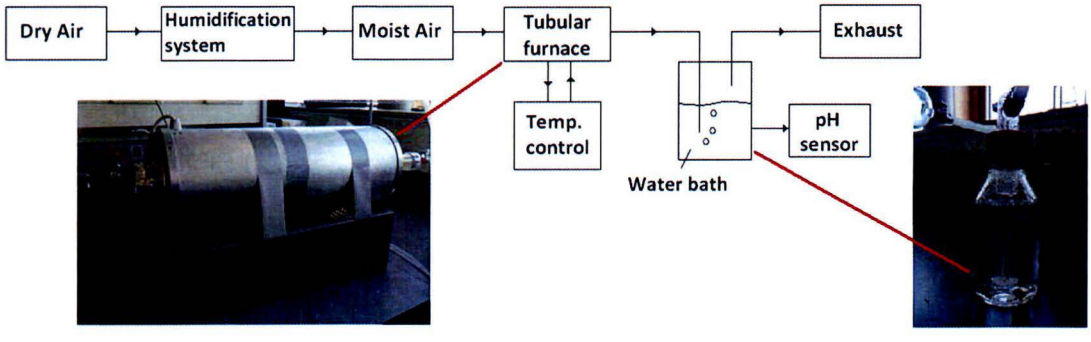

Figure 16: Schematic overview of the Tubular Furnace system setup

A schematic overiew of the cross-section of the tubular furnace with a close-up of the crucible containing $MgCl_2.6H_2O$ is given in the figure below:

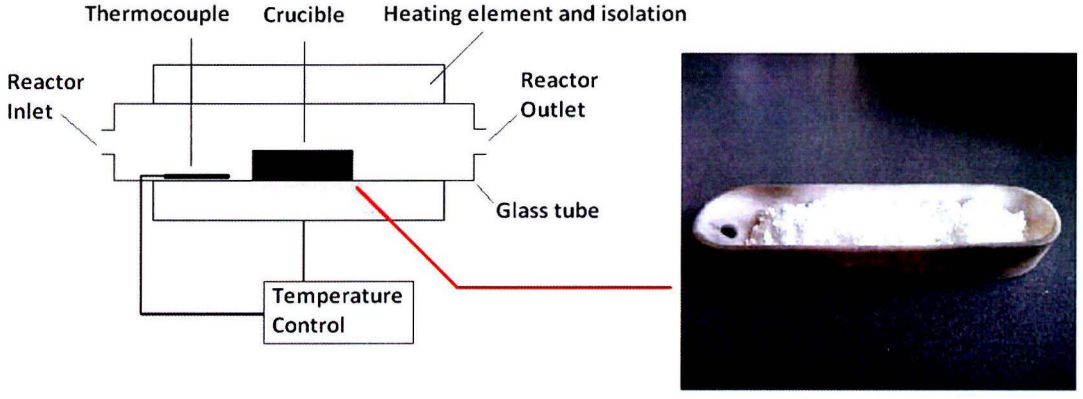

Figure 17: Schematic overview of the cross-section of the tubular furnace with a close-up of the crucible

A schematic overview of the humidification system is given in the following figure:

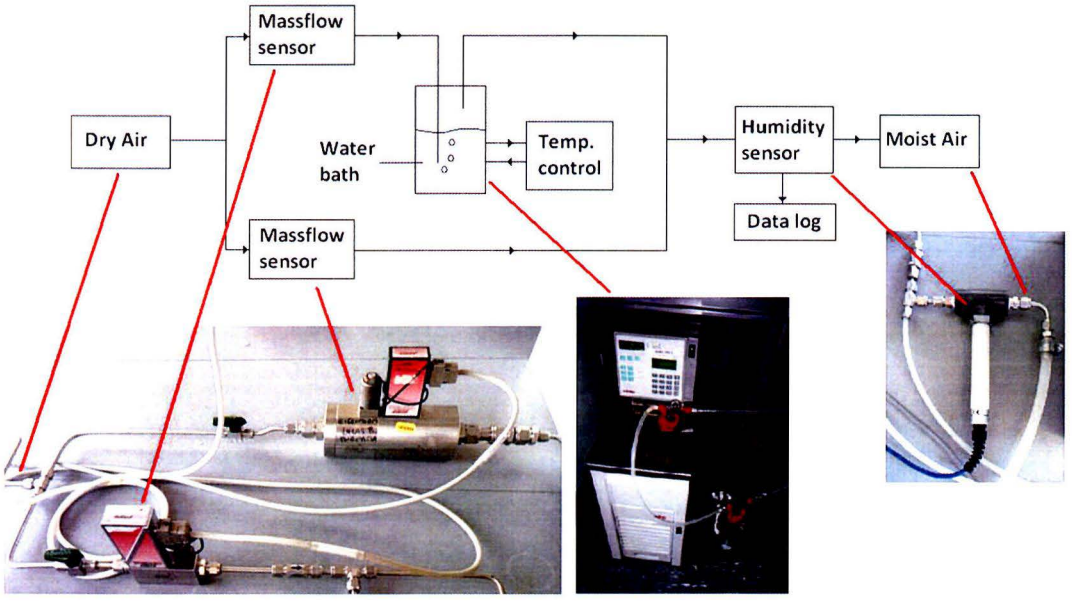

Figure 18: Schematic overview of the humidification system setup

Dry air provided by a compressed air network enters the humidification system and is subsequently split up. One part of the dry air goes through a water bath at 10°C to 12°C in which the water vapor pressure is increased. The initial dry air and the humidified air are then mixed to obtain a water vapor pressure equal to 13 mbar before they are introduced in the tubular furnace. The water vapor pressure in the system can be controlled by changing the flow ratio between the dry air and the moist air. By using this parallel flow setup, one has a flexible and fast control of the water vapor pressure.

A Pico humidity probe, as shown in Figure 18, measures the humidity and temperature of the air, from which the water vapor pressure can be calculated. The connection of the humidity probe with

the air pipes contains some small leakages, which result in a small pressure drop in the system. The total air flow through the system is therefore set to 400 ml/min, which is the practical minimum air flow required to overcome the pressure drop and to drive the air through the two water baths.

Each experiment started with an activation cycle, in which the salt hydrate is heated up to 130°C (with a heating rate of 100°C/hr) and then cooled to 40°C. This activation cycle introduces cracks in the material which improve the diffusion of water vapor and therefore increase the reaction kinetics.
After the activation cycle, the furnace is heated up again to 110-150°C (at a heating rate of 100°C/hr) at a p_{H2O} of 13 mbar, after which the temperature in the furnace was kept constant at this level for several days. The temperature profile inside the reactor is shown in figure A2-1 in appendix A2.
At a furnace temperature of 110°C, the $MgCl_2.6H_2O$ is partially dehydrated to $MgCl_2.2H_2O$. This temperature level is too low for further dehydration of the $MgCl_2.2H_2O$ into $MgCl_2.H_2O$, preventing the competitive effect of multiple dehydration/decomposition reactions. At 150°C however, further dehydration of $MgCl_2.2H_2O$ to $MgCl_2.H_2O$ is possible at 13 mbar p_{H2O}.
Overhydration, as discussed in paragraph 2.2.1, was prevented by keeping the minimum temperature in the furnace above 30°C.

The amount of salt in the furnace was relatively large, ~10 gram, which made it possible to take samples of the material during the experiment. These samples were used for XRD, SEM-EDAX, pH and weight measurements in order to observe the structural properties of the material.
For the experiments, a water bath was used containing demineralized water in combination with a pH sensor to measure the possible formation of HCl in the dehydration/hydrolysis process of $MgCl_2.6H_2O$. The exhaust flow of the tubular furnace passes through the water bath which decomposes the HCl into H^+ and Cl^-. The decrease in the pH value can then be used to determine the amount of HCl formed. A diffuser, as shown in Figure 19, was used at the inlet of the water bath in order to produce multiple small bubbles, which will improve the solution process of HCl(g) into $H^+(aq)$ and $Cl^-(aq)$. This will reduce the amount of HCl which passes through the water bath without being absorbed.

Figure 19: Close-up of the diffuser used in the water bath

The effect of diffusion of reaction participants on the dehydration and hydrolysis of $MgCl_2.6H_2O$ was analyzed by changing the sample mass and thereby the sample thickness. The sample mass was hereto varied between 5 and 15 gram.
Finally, the air flow through the reactor was varied between 400 ml/min and 2000 ml/min in order to analyze the effect of water vapor supply and removal on the dehydration and hydrolysis of the salt hydrate. An air flow of 400 ml/min is a practical minimum in order to overcome a certain pressure drop in the system as described earlier. An air flow of 2000 ml/min is on the other hand a practical maximum in order to limit additional leakages as a result of an increasing pressure in the system.

4.2 Characterization of $MgSO_4.7H_2O$: High Pressure DSC

The dehydration and rehydration reactions of $MgSO_4.7H_2O$ are analyzed by means of an experimental setup containing a high pressure differential scanning calorimeter and a humidification system similar to the one described in the previous chapter.

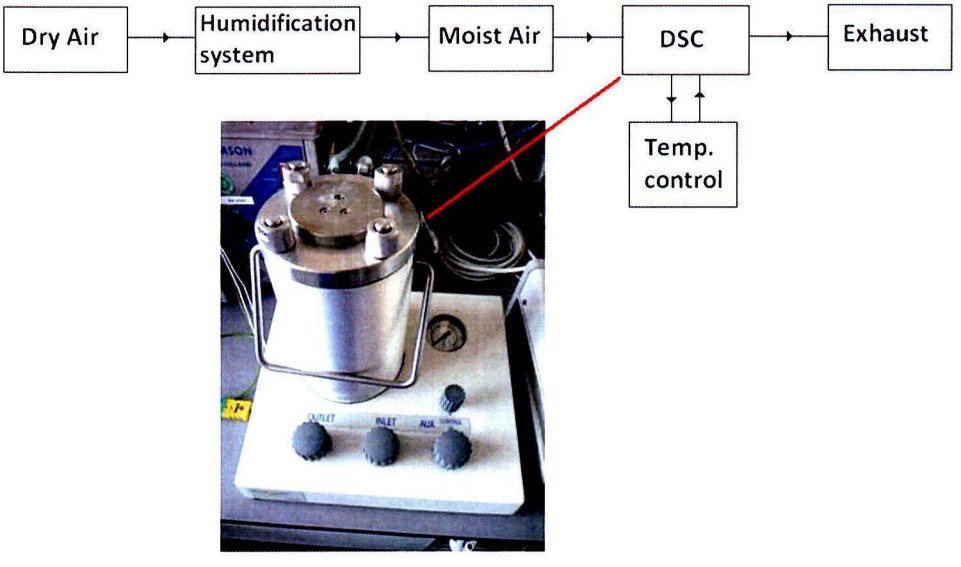

Figure 20: Schematic overview of the High Pressure DSC system setup

The humidification system works in a similar way as described in the previous chapter: dry air is humidified by a water bath and afterwards introduced in the DSC reactor. However, in this setup are also insulation and heating elements incorporated, in order to reduce coldspots to prevent condensation. This makes it possible to operate at higher water vapor pressures.

The dehydration of $MgSO_4.7H_2O$ will be studied at water vapor pressures varying between 8 mbar and 70 mbar. The critical water vapor pressure for $MgSO_4.7H_2O$ is equal to 8 mbar, as described in paragraph 2.2.2. The reaction rate corresponding to this p_{H2O} will then be at a minimum. The water

vapor pressure cannot be increased to values above 70 mbar due to practical limitations in the system setup. The Pico humidity probe must not be exposed to temperatures above 70°C, which is thus the upper temperature limit in the air pipes. In order to stay within a safe margin, the maximum operating temperature will be limited to 60°C in the air pipes. In addition, the maximum flow allowed flow through the DSC during a measurement, and thus through the water bath, is equal to 100 ml/min. These two boundary conditions result in a maximum achievable p_{H2O} of 70 mbar.

The temperature program used to heat the samples in the DSC varies for different measurements. The maximum temperature used is always equal to 150°C, which is assumed to be the upper temperature limit for seasonal heat storage. The minimum required temperature to prevent overhydration has to be adjusted according to Figure 7, when changing the p_{H2O} in the system. An increasing water vapor pressure means that the minimum temperature in the DSC also has to be increased. At 8 mbar this minimum temperature is 5°C whereas at 70 mbar the minimum temperature required to prevent overhydration must be at least 40°C.
The heating rate used will be varied between 1, 2 and 5 °C/min, in order to be able to calculate the activation energy according the FWO method, as described in chapter 3.2.
The sample mass will be equal to about 10 mg for each measurement and is contained in a small aluminum cup. The moist air is again driven over the sample, instead of through the sample.

4.3 Packed Bed Reactor

The Packed Bed Reactor (PBR) is used to simulate the practical operating conditions in a seasonal sorption heat storage. Moist air with a controlled water vapor pressure is hereto driven directly through the sample in the reactor. The reactor is 7 cm in diameter and 17 cm in height, with a total volume of 0,65 dm^3. The amount of salt hydrate that can be stored in this volume is equal to about 700 gram.

Figure 21 gives a schematic overview of the PBR system setup.

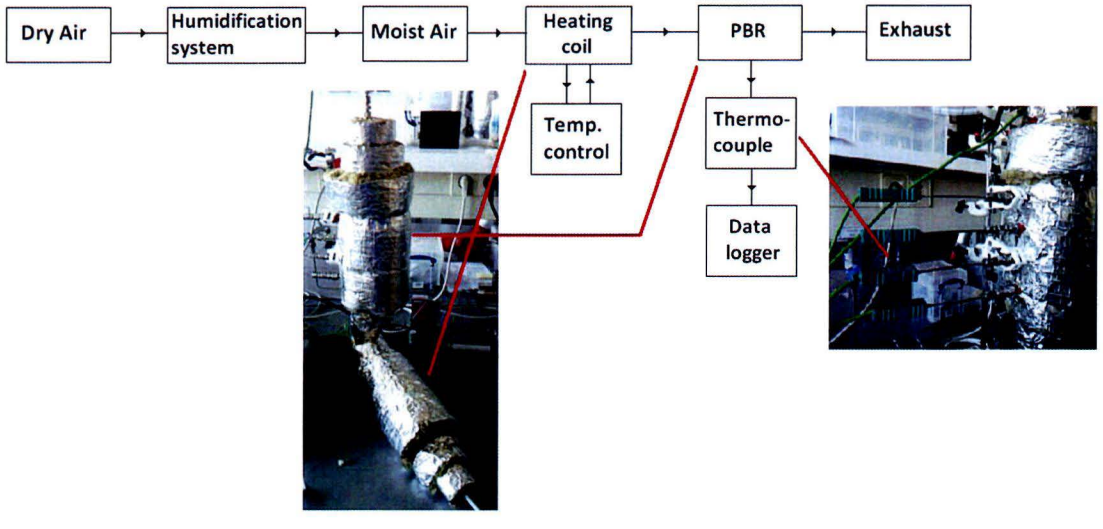

Figure 21: Schematic overview of the Packed Bed Reactor system setup

A schematic overview of the cross-section of the packed bed reactor is given in the following figure:

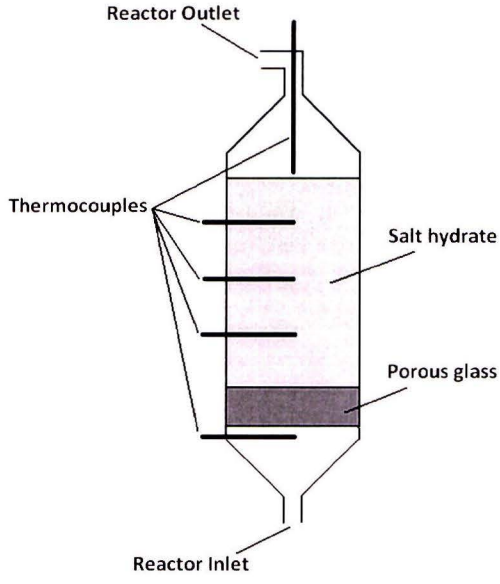

Figure 22: Schematic overview of the cross-section of the packed bed reactor

Dry air is humidified in a similar way as described in chapter 4.1. The moist air is subsequently driven through the reactor where the dehydration or rehydration of the salt hydrate takes place. The heat required for dehydration is generated by a heating coil, which heats the moist air to temperatures varying between 100°C and 150°C (depending on the salt hydrate used), before the air is introduced in the reactor.

The heating power during rehydration of the salt hydrate will be studied by means of temperature variations in the bed. These temperatures will be measured by thermocouples which are placed at different heights in the bed (at 25%-, 50%-, 75% bed height), as well as in the inlet and outlet of the reactor. In order to study the rehydration process, the material has to be dehydrated first and subsequently cooled to room temperature without any mass flow through the bed, after which it is rehydrated with humid air.
The heating power will be studied for varying mass flow and reactor inlet temperatures. The mass flow will be varied between 20 liter/min and 50 liter/min. A mass flow of 50 liter/min is the practical upper limit of this setup, due to the dimensions of the water bath. Operating the setup at a mass flow above 50 liter/min will result in direct transport of water from the water bath through the pipes and reactor. A mass flow of 20 liter/min is a practical minimum, for the dehydration at this mass flow will take several days.
The reactor inlet temperature will be varied between 30°C and 50°C during rehydration. A minimum temperature of 30°C will be maintained in order to prevent overhydration as discussed in paragraph 2.2.1. A maximum inlet temperature of 50°C will be maintained, for this will be the assumed practical limit for a seasonal sorption heat storage setup in which the reactor outlet flow preheats the reactor inlet flow as discussed in paragraph 2.2.1. The abovementioned parameters will be varied in order to obtain an optimal heating power during rehydration of the salt hydrates.

4.4 Experimental setup overview

The table below gives an overview of the prementioned characteristics of the different experimental setups used.

Experimental Setup	Use	Temperature (°C)	Mass	Mass flow	Water vapor pressure	Activation step
Tubular Furnace	**Characterization of $MgCl_2.6H_2O$ (hydrolysis)**	**Isothermal: 110/130/150**	**Varying: 5/10/15 gram**	**Varying: 400/1000 ml/min**	**13 mbar**	**yes**
HPDSC	Characterization of $MgSO_4.7H_2O$ (kinetics of reaction)	Dynamic: 30°C to 150°C	10 mg	100 ml/min	Varying 8/13/20/30/ 50/60/70 mbar	no
Packed Bed Reactor	**Characterization of $MgSO_4.7H_2O$ and $MgCl_2.6H_2O$**	**Isothermal; Dehydration: 130 Rehydration: 30/40/50**	**700 gram**	**Varying: 20/35/50 L/min**	**$MgCl_2.6H_2O$: 13 mbar $MgSO_4.7H_2O$; Varying: 13/50 mbar**	**yes**

Table 3: Characteristics of the different experimental setups used

5 Results and Discussion

5.1 Characterization of $MgCl_2.6H_2O$

In this chapter, the characteristics of $MgCl_2.6H_2O$ will be discussed based on the experiments performed in the tubular furnace. Hereto, the hydrolysis of $MgCl_2.6H_2O$ will be studied at different temperatures (paragraph 5.1.1), different sample sizes (paragraph 5.1.2) and different massflow rates (paragraph 5.1.3).

5.1.1 Dehydration of $MgCl_2.6H_2O$ at different operating temperatures

The development of the sample mass with respect to time at different operating temperatures in the tubular furnace is shown in the following figure:

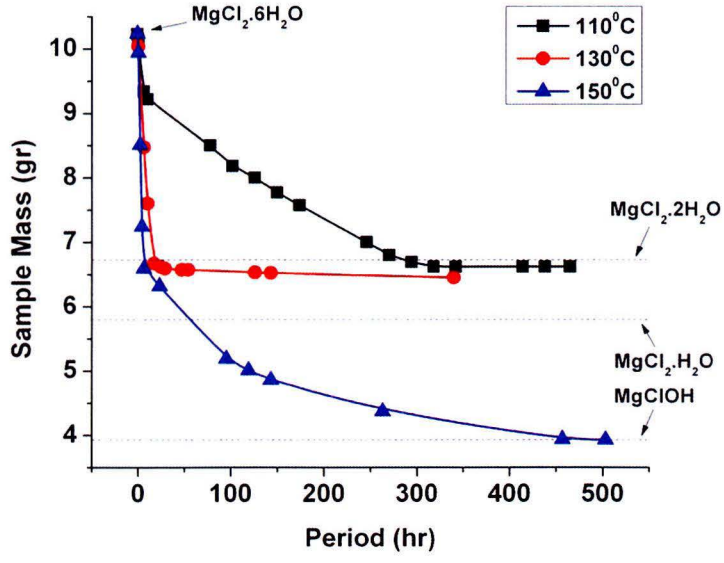

Figure 23: Mass measurements of the dehydration of $MgCl_2.6H_2O$ at different temperatures

The salt hydrate is initially fully hydrated and has an initial mass of about 10 gram, as can be seen from the figure above. At a reactor temperature of 110°C it takes about 350 hours for the sample to dehydrate to $MgCl_2.2H_2O$ after which the sample mass remains stable. The theoretical mass of the $MgCl_2.2H_2O$ is equal to 6,73 gram, based on the initial mass of the $MgCl_2.6H_2O$ of 10 gram. From Figure 23 it can be seen that the mass of the sample, after 350 hours of dehydration at 110°C, is slightly less than this theoretical mass. Since the sample is not dehydrated further to $MgCl_2.H_2O$ at this temperature, this indicates that the mass difference could be a result of hydrolysis in the sample.

The dehydration of $MgCl_2.6H_2O$ to $MgCl_2.2H_2O$ takes about 20 hours at a reactor temperature of 130°C. At this temperature, the sample mass does not remain stable after 20 hours, but decreases

slowly over time. This could mean that further dehydration and/or hydrolysis is taking place in the period of 20 to 340 hours. From the equilibrium curves in Figure 12 it can be seen that the 2-1 dehydration is exactly in equilibrium at a water vapor pressure of 13 mbar and a temperature of 130°C. This implies that at these given conditions, the dehydration of $MgCl_2.2H_2O$ to $MgCl_2.H_2O$ is taking place. But this doesn't rule out the possibility of additional hydrolysis in the sample at these conditions.
The theoretical mass of MgClOH is 3,93 gram based on the initial mass of the $MgCl_2.6H_2O$. This theoretical mass corresponds to the sample mass measured after 450 hours at a reactor temperature of 150°C, as can be seen from Figure 23. This implies that full hydrolysis is achieved after this period at this given temperature.

In order to quantify the possible hydrolysis during the dehydration of $MgCl_2.6H_2O$, additional XRD, SEM-EDAX and pH measurements were performed. The results of these XRD measurement are shown in the following figure:

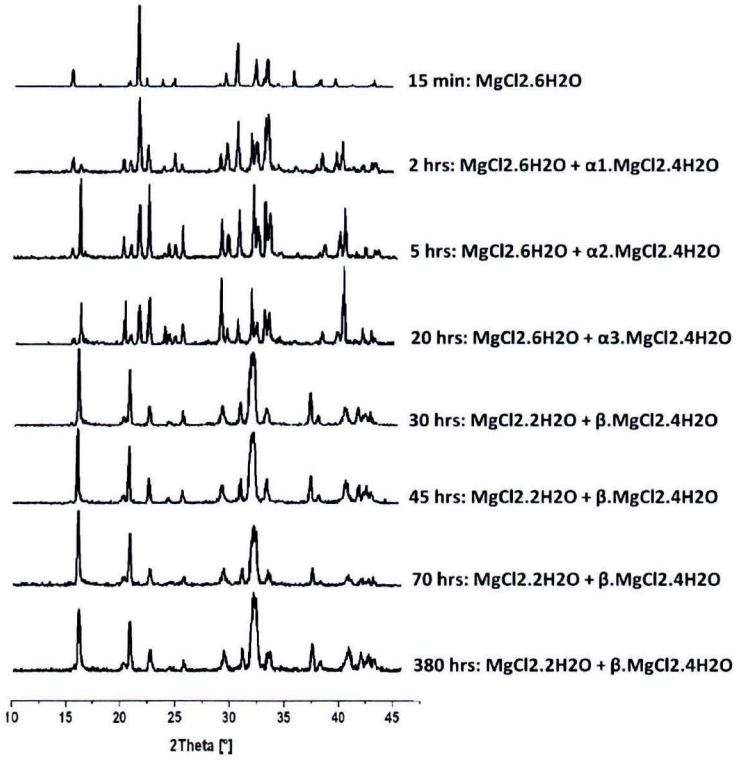

Figure 24: XRD measurement of the dehydration of $MgCl_2.6H_2O$ at 13 mbar and 130°C

For these XRD measurements, samples were taken from a crucible containing the salt hydrate, each after a different dehydration period in the tubular furnace. From Figure 24 it can be seen that the initial $MgCl_2.6H_2O$ is dehydrated to mainly $MgCl_2.2H_2O$ with a certain mass fraction β of $MgCl_2.4H_2O$ in about 30 hours at 130°C. The further dehydration to $MgCl_2.H_2O$ cannot be observed in the XRD measurements, not even after 380 hours. However, from Figure 24 it can be concluded that the presence of a measurable mass fraction of $MgCl_2.4H_2O$ in the sample is unlikely after 380 hours of dehydration at 130°C, since the sample mass is less than the theoretical mass of $MgCl_2.2H_2O$ after

this period. Based on this observation it was concluded that the sample was starting to rehydrate during the preparation process for the XRD measurement, making the XRD measurements inaccurate. However, rehydration does not affect the amount of MgClOH present in the sample. The presence of MgClOH was nevertheless not observed in the XRD results.

SEM-EDAX measurements were used to determine the Cl/Mg ratio in dehydrated $MgCl_2.6H_2O$ samples. A Cl/Mg ratio equal to 2 indicates that no hydrolysis has taken place while a Cl/Mg ratio equal to 1 implies complete hydrolysis. Figure 25 shows the SEM-EDAX results for the dehydration of $MgCl_2.6H_2O$ after 400 hours at 130°C. For this measurement, 12 samples were taken at different locations in the crucible.

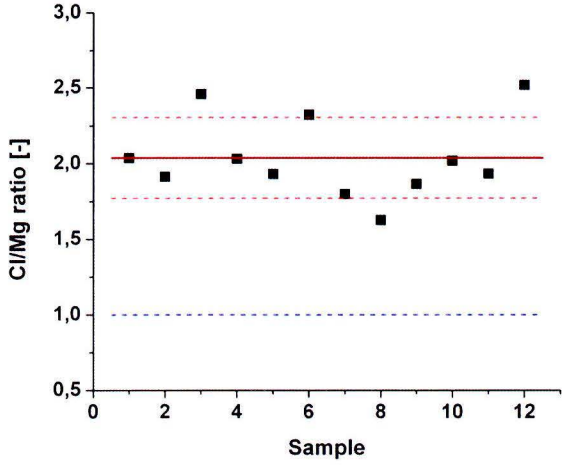

Figure 25: SEM-EDAX measurements for the dehydration of $MgCl_2.6H_2O$ after 400 hours at 130°C

From Figure 25 it can be seen that the average Cl/Mg ratio is equal to 2,04 (red solid line). The standard deviation in these measurement (red dashed line) state that there is a 34,1% chance that the Cl/Mg ratio lies between 2,04 and 1,77 which means that there is a 34,1% chance that hydrolysis has taken place in the sample. The standard deviation in these measurement is thus too large to allow an accurate quantification of the possible hydrolysis. The blue dashed line represent the value for the Cl/Mg ratio at which complete hydrolysis has taken place.

pH measurements were used to determine the possible formation of HCl during the hydrolysis/dehydration of $MgCl_2.6H_2O$. For these experiments, a water bath was used in combination with a pH sensor as described in chapter 4.1. The results of these measurements are shown in the following figure:

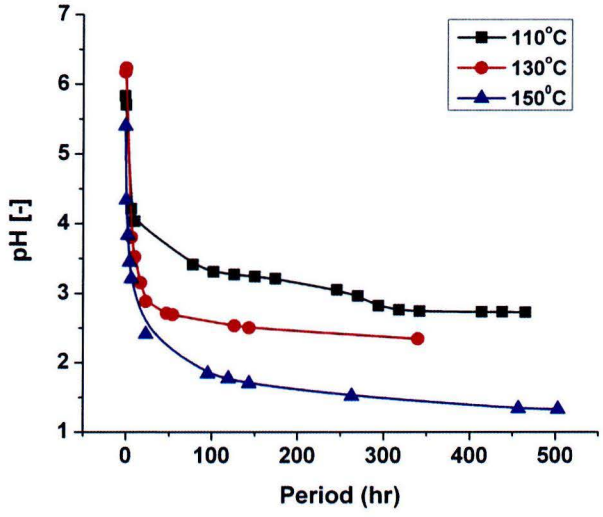

Figure 26: pH measurement for the dehydration of $MgCl_2.6H_2O$ at 13 mbar p_{H2O} and at different furnace temperatures

Figure 26 shows a clear decrease in the pH value of the water bath with respect to time, indicating that hydrolysis is taking place at all three furnace temperatures. The initial pH of the demineralised water bath is equal to about 6, which is a result of the formation of carbonic acid in demineralised water. The highest hydrolysis at these furnace temperatures is achieved at 150°C. This is conformal with the equilibrium curves presented in Figure 5 in paragraph 2.2.1. From Figure 26 it can also be seen that the formation of HCl and thus the hydrolysis doesn't increase further after 350 hours at 110°C. This is consistent with the trend of the mass development as presented in Figure 23. From these observations it can be concluded that at a furnace temperature of 110°C, the hydrolysis mainly occurs during the dehydration of the material. This implies that at 110°C, the hydrolysis is limited because the material can't be dehydrated further to $MgCl_2.H_2O$. At a furnace temperature of 130°C and 150°C, the dehydration step of $MgCl_2.2H_2O$ to $MgCl_2H_2O$ is possible, which also results in additional hydrolysis.

The amount of HCl formed is used to determine the amount of mass decomposed. At 0% no hydrolysis has taken place whereas at 100% complete hydrolysis has occurred. These findings are presented in figure below:

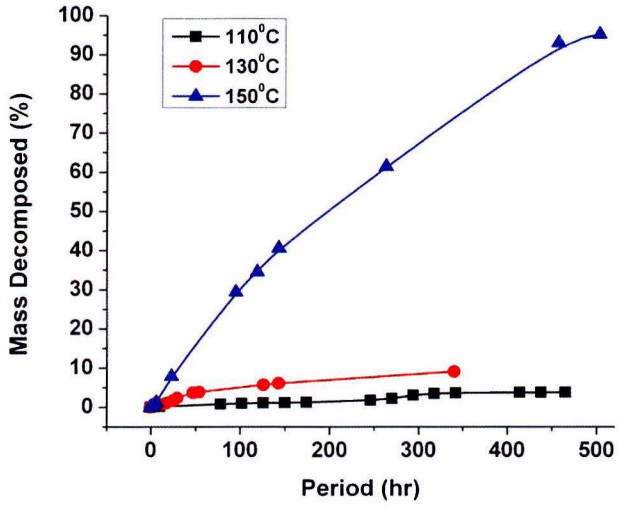

Figure 27: Mass decomposed at different furnace temperatures and at 13 mbar p_{H2O}

Figure 27 clearly shows the difference in the hydrolysis reaction rate between the different furnace temperatures. After 500 hours at 150°C the material has decomposed completely, which is consistent with the findings presented in Figure 23. The mass decomposition is steady at about 4% after 350 hours at 110°C. After this period no more decomposition occurs which is conformal with the mass development in Figure 23. The mass decomposition at 130°C increases steady with time and complete decomposition would take several hundredths of hours at this rate.

The mass decomposition as a function of the sample mass in shown in the figure below.

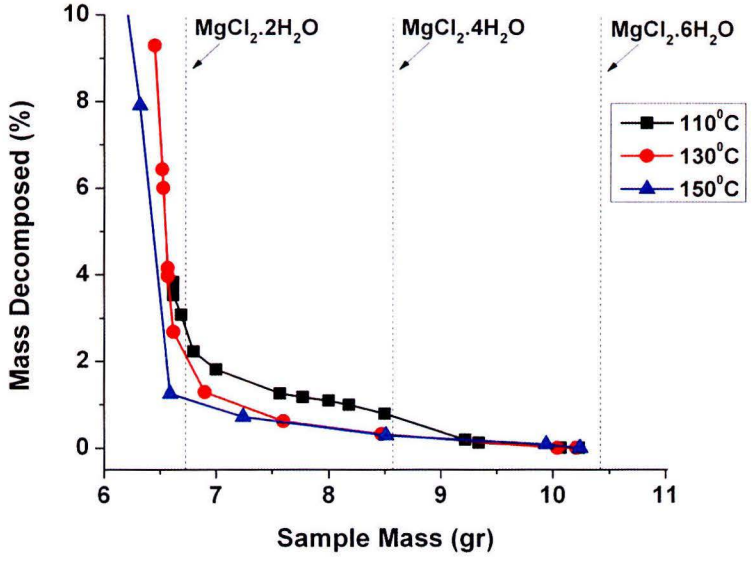

Figure 28: Mass decomposed as a function of the sample mass at different furnace temperatures and at 13 mbar p_{H2O}

From Figure 28 it can clearly be seen that hydrolysis occurs in the whole dehydration range of $MgCl_2.6H_2O$ to $MgCl_2.2H_2O$. Even in the 6-4 dehydration can a mass decomposition be observed. The highest decomposition occurs however after $MgCl_2.2H_2O$ has formed, as can be seen from the sharp increase after this point.

Both the hydrolysis and the dehydration occur fastest at a furnace temperature of 150°C, as shown in Figure 23 and Figure 27. This results however in the slowest decomposition trend in the dehydration range of $MgCl_2.6H_2O$ to $MgCl_2.2H_2O$ with respect to a furnace temperature of 110°C and 130°C, as shown in Figure 28. The highest mass decomposition is achieved at 110°C in this range. This can be a result of the much larger dehydration period at this furnace temperature. At 110°C, the dehydration of $MgCl_2.6H_2O$ to $MgCl_2.2H_2O$ takes about 350 hours, while the same dehydration takes about 10 and 20 hours at 150°C and 130°C respectively.

From Figure 28 it can again be seen that the mass decomposition is limited at about 4% at a furnace temperature of 110°C. The sample is then dehydrated to $MgCl_2.2H_2O$. However, at this same point the mass decomposition at a furnace temperature of 130°C and 150°C is equal to about 2.5% and 1.2% respectively. From these observations can be concluded that a limitation of the mass decomposition of 1.2% per cycle is possible, when the heat storage system is well regulated with respect to temperature distributions within the reactor in combination with accurate observations of the dehydration state.

5.1.2 Dehydration of $MgCl_2.6H_2O$ at different layer thickness

During the measurements in the tubular furnace, the sample is contained within a crucible (Figure 17) over which the air flow is driven. In a packed bed reactor however, the air flow is driven through the sample. In order to get a better understanding of the hydrolysis of $MgCl_2.6H_2O$ when applied in a packed bed reactor, the sample mass and thereby the sample layer thickness is varied in the crucible. The sample mass was varied between 5, 10 and 15 gram which results in a varying layer thickness of 0.5, 1.0 and 1.5 cm.

The mass decomposition as a function of time at different layer thickness is shown in Figure 29. For these measurements, the furnace temperature was set to 130°C and the water vapor pressure to 13 mbar. From Figure 29 it can be seen that the sample decomposes the fastest at the smallest layer thickness and that an increasing layer thickness results in a decreasing hydrolysis rate. This implies that diffusion plays an important part in the hydrolysis process, when the air flow is driven over the sample. A larger sample thickness may thus result in a larger p_{HCl} in the sample, thereby limiting the hydrolysis rate, as discussed in paragraph 2.2.1. This also implies that, with respect to these measurements, the hydrolysis rate will be higher in a packed bed reactor, due to the increased diffusion in the bed.

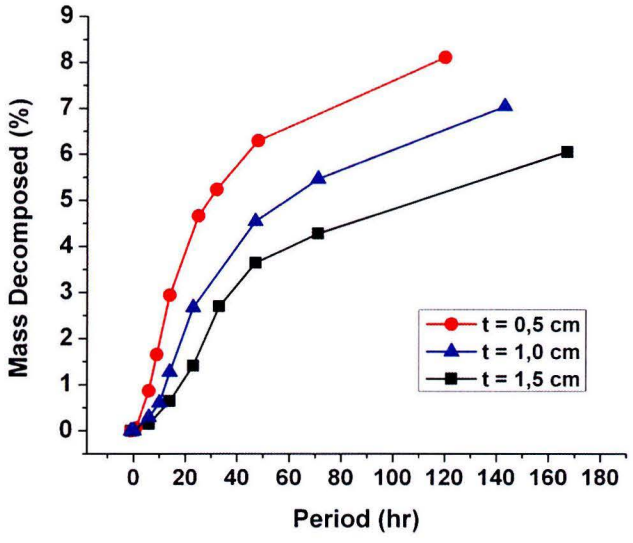

Figure 29: Mass decomposed as a function of time at different sample layer thickness at a furnace temperature of 130°C and 13 mbar p_{H2O}

The dehydration rate also changes as a results of a changing layer thickness, as can be seen from the figure below. The decrease in the mass occurs the fastest at the smallest layer thickness, at a furnace temperature of 130°C and 13 mbar p_{H2O}. This implies that diffusion also plays an important part in the dehydration of the sample. A smaller sample thickness decreases the p_{H2O} in the sample and thereby increases the dehydration rate. At a furnace temperature of 130°C, all three measurements converge after dehydration to $MgCl_2.2H_2O$, indicating that further dehydration takes place at a much slower rate for all three samples.

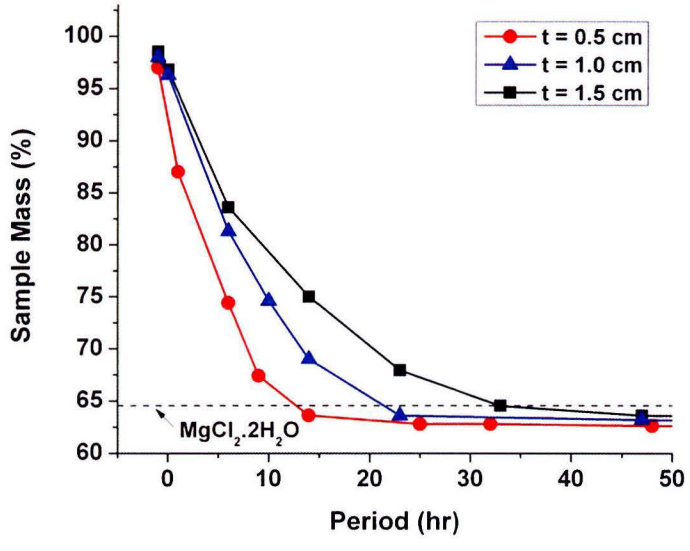

Figure 30: Sample mass as a function of time at different layer thickness at a furnace temp. of 130°C and 13 mbar p_{H2O}

Both the hydrolysis- and dehydration rate increase for a decreasing sample thickness, due to the decrease in the vapor pressure in the sample. This results in the following relation between the mass decomposition and the sample mass:

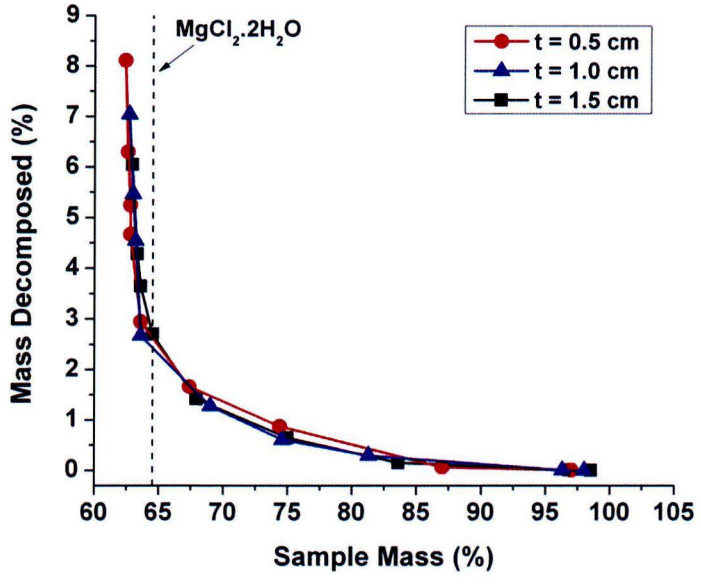

Figure 31: Mass decomposition as a function of the sample mass at different layer thickness at a furnace temperature of 130°C and 13 mbar p_{H2O}

From Figure 31 it can be seen that all three curves follow the same trend. Regardless of the sample layer thickness, the material has the same mass decomposition after dehydration to $MgCl_2.2H_2O$ at 130°C. The increase in the dehydration rate and the additional increase in the hydrolysis rate as a result of a smaller layer thickness thus compensate each other. This implies that the mass decomposition in a packed bed reactor can also be limited at around 2.5% per dehydration-rehydration cycle at 130°C and 13 mbar p_{H2O}.

5.1.3 Dehydration of $MgCl_2.6H_2O$ at different massflow rates

The massflow of the moist air is varied between 0,4 L/min, 1 L/min and 2 L/min in order to analyze the effect of the massflow on the hydrolysis and dehydration rate. The corresponding results are shown in the figure below:

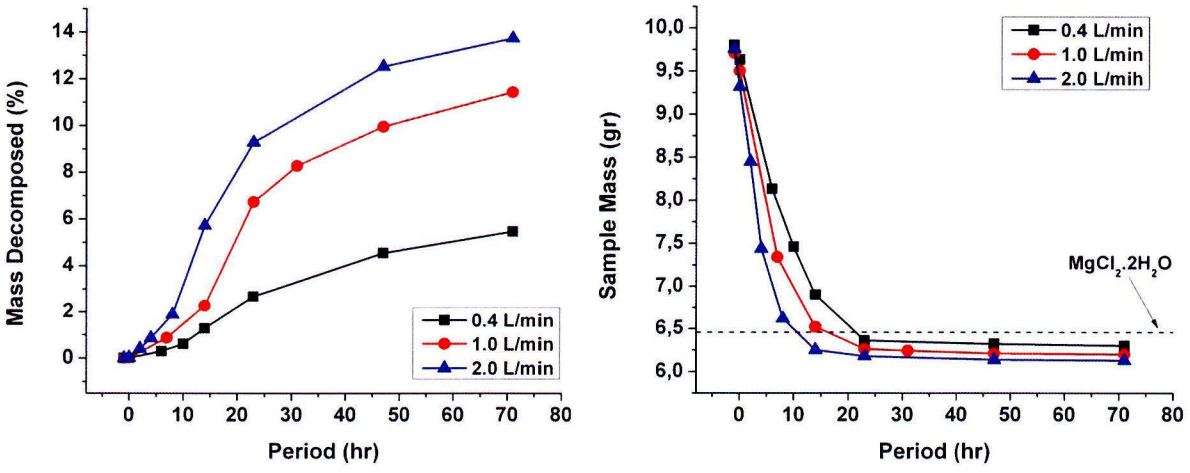

Figure 32: Mass decomposed (left) and sample mass (right) as a function of time at different air mass flow rates, at a furnace temperature of 130°C and 13 mbar p_{H2O}

From Figure 32 it can be seen that both the hydrolysis- and dehydration rate increase with an increasing massflow rate. This can be explained by the decrease of the vapor pressure in the bed with an increasing massflow rate and thus an increasing transport rate. These findings correspond to the findings at different layer thickness' as discussed in the previous paragraph, indicating that the hydrolysis- and dehydration rate can be increased by increasing the massflow rate and/or by decreasing the sample layer thickness.
The mass decomposition as a function of the sample mass is shown in the following figure:

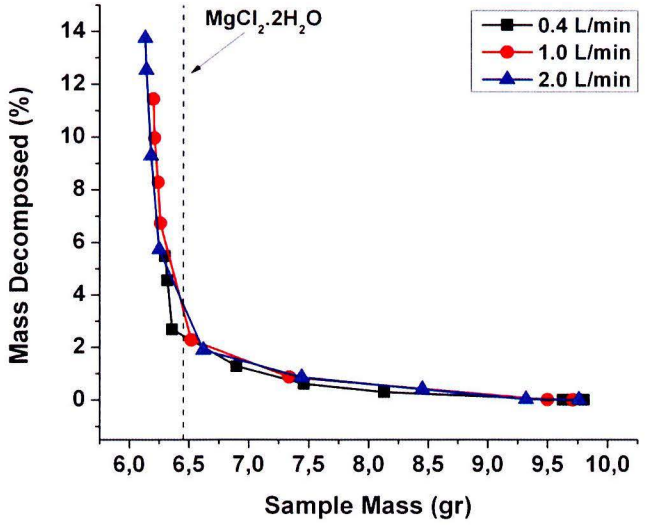

Figure 33: Mass decomposition as a function of the sample mass at different massflow rates at a furnace temperature of 130°C and 13 mbar p_{H2O}

From Figure 33 it can be seen that the curves overlap, which is again consistent with the findings presented in the previous paragraph. The increase in the hydrolysis rate is compensated by the increase in the hydrolysis rate, resulting in an identical mass decomposition after dehydration to $MgCl_2.2H_2O$. The hydrolysis rate increases sharply after the material is dehydrated to $MgCl_2.2H_2O$, which is consistent with the findings presented in Figure 28 and Figure 31. From the results presented in this chapter, it can be concluded that the mass decomposition with respect to the sample mass in only influenced by the furnace temperature. The mass decompositions at varying layer thickness and varying massflow rate all coincide in the dehydration range of $MgCl_2.6H_2O$ to $MgCl_2.2H_2O$.

5.2 Characterization of $MgSO_4.7H_2O$

In this chapter, the characteristics of $MgSO_4.7H_2O$ will be discussed based on the results of the HPDSC measurements. Hereto, the dehydration and rehydration will be analyzed for different water vapor pressures.
The dehydration characteristics of $MgSO4.7H_2O$ will be discussed in paragraph 5.2.1 and 5.2.2 and the rehydration characteristics in paragraph 5.2.3.

5.2.1 Dehydration of $MgSO_4.7H_2O$

The results of the HPDSC measurements for the dehydration of $MgSO_4.7H_2O$ at 13 mbar p_{H2O} and a heating rate of 1°C/min are shown in Figure 34. The DSC signal shows the rate of heat absorbed [mW/mg] by the sample as a function of the sample temperature T_s [°C]

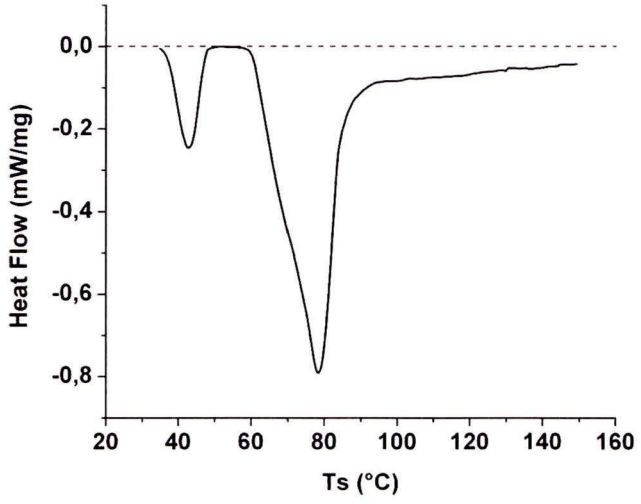

Figure 34: DSC signal for dehydration of $MgSO_4.7H_2O$ at 13 mbar p_{H2O} and 1°C/min heating rate

Figure 34 shows two clear dehydration peaks, which are consistent with the findings of Ferchaud et al. presented in Figure 9 in paragraph 2.2.2. The first peak in the temperature range of 35°C to 50°C corresponds to the dehydration of $MgSO_4.7H_2O$ to $MgSO_4.6H_2O$ (7-6 dehydration) in which one water molecule is released. The second peak in the temperature range of 60°C to 150°C corresponds to the dehydration of $MgSO_4.6H_2O$ to $MgSO_4.H_2O$ (6-1 dehydration). From Figure 34 it can also be seen that the two dehydration reactions are separated by a steady state at 50°C to 60°C in which no heat is absorbed by the salt hydrate.
The tail effect in the temperature range of 90°C to 150°C is a results of amorphization of the material, as also discussed in paragraph 2.2.2. The transition from a crystalline phase towards an amorphous phase start at around 60°C and is complete at around 80°C. The disordered amorphous structure reduces the diffusion of water vapor through the material, thereby limiting the water

vapor removal during dehydration. This reduction in the water vapor removal results in a slow absorption of heat which can be observed in the temperature range of 90°C to 150°C.
The tail effect can also be explained by the local variations in the bonding energy of the H_2O molecules as a result of the disordered amorphous structure. These local variations in the bonding energy result in a range of ΔH for further dehydration in the salt hydrate.

The rate of heat absorbed by the sample changes for a varying water vapor pressure between 8 and 70 mbar, as can be seen from Figure 35. The peak value of the heat flow increases with an increasing p_{H2O} up to a maximum at a p_{H2O} of 50 mbar. Increasing the water vapor pressure further, results again in a decrease of the maximum heat flow.
The onset temperature also shifts with increasing water vapor pressure due to thermodynamics, as described by equation 6 in chapter 3.1. Increasing the p_{H2O} results in a consistent increase of the equilibrium temperature, T_{eq}, and thus in an increase of the onset temperature, T_{onset} for both dehydration reactions.
The tail effect is still present in the temperature range of 90°C to 150°C, even at a water vapor pressure of 70 mbar as can be seen from Figure 35. This is an indication that the formation of the amorphous phase is thus not prevented.

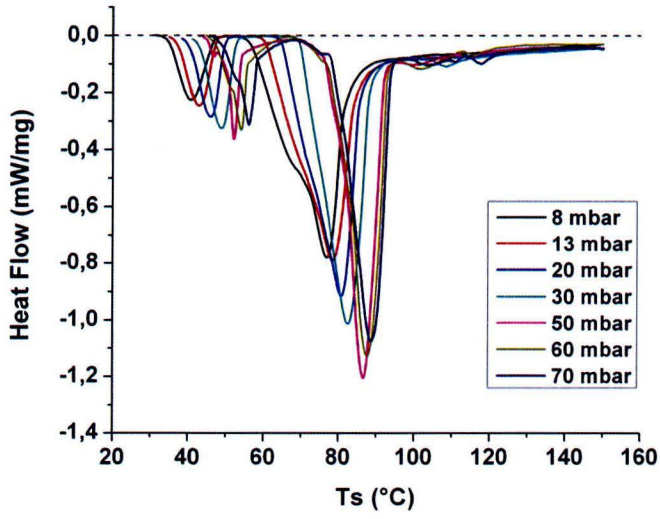

Figure 35: DSC signal for dehydration of $MgSO_4.7H_2O$ for different p_{H2O} and 1°C/min heating rate

The full width at half maximum (FWHM) changes with an increasing water vapor pressure as can be seen from Figure 36. The trend in the FWHM is inversely proportional to the trend of the maximum heat flow in Figure 35. The FWHM decreases up to a water vapor pressure of 50 mbar indicating that the heat is absorbed over a smaller period of time and thus that the reaction is proceeding at a faster rate. At a water vapor pressure above 50 mbar, the FWHM increases again, indicating that the kinetics of reaction are again declining.

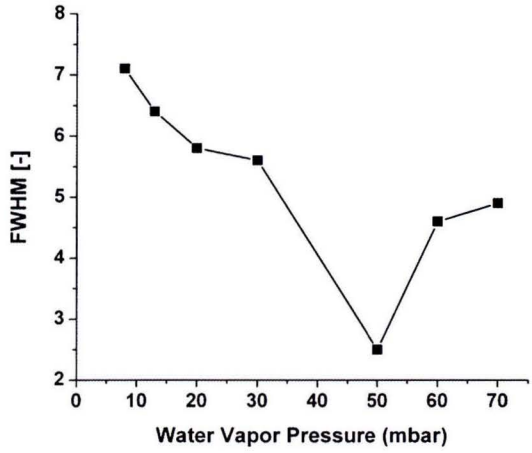

Figure 36: FWHM for different p_{H2O} for the dehydration of $MgSO_4.7H_2O$

The mass fraction reacted is calculated from the DSC signal using the method described in paragraph 3.3.1. The mass fraction reacted is equal to zero when the material is fully hydrated ($MgSO_4.7H_2O$) and equal to 1 when the material is dehydrated to $MgSO_4.H_2O$. Figure 37 shows the mass fraction reacted as a function of the sample temperature. The two dehydration reactions can be distinguished from the trend in Figure 37. The first dehydration reaction occurs in the temperature range of 35°C to 60°C whereas the second dehydration takes place in between 60°C and 150°C. The transition between the two dehydration reactions shows a steady state (i.e. a region in which the mass fraction reacted does not increase) for the reactions at 8, 13, 20 and 30 mbar. However, the mass fraction reacted shows a continuous increase for the dehydration reactions performed at a p_{H2O} of 50 mbar and higher. This implies that the two dehydration reactions merge in the transition phase, and thus that the first dehydration reaction is still ongoing when the second dehydration reaction is initiated.

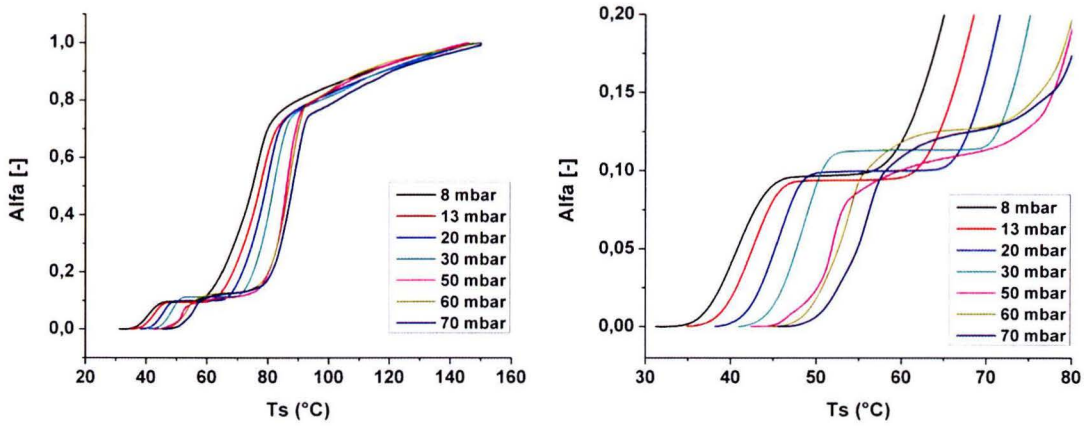

Figure 37: Mass fraction reacted as a function of the sample temperature for varying p_{H2O} and 1°C/min heating rate for the dehydration of $MgSO_4.7H_2O$ (left) and close-up of the first part of dehydration (right)

The reaction rate is calculated by taking the time derivative of the mass fraction reacted, as described in paragraph 3.3.1. Figure 38 shows the reaction rate as a function of the sample temperature for different values of the water vapor pressure and at a heating rate equal to 1°C/min.

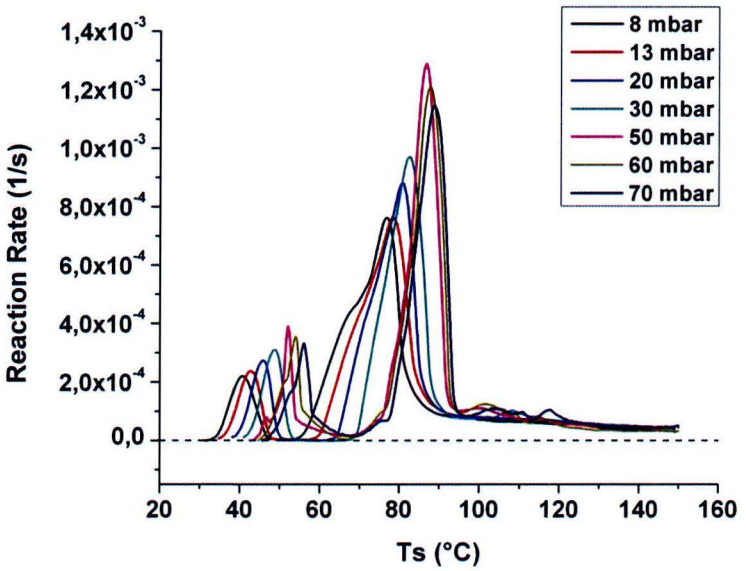

Figure 38: Reaction rate for dehydration of $MgSO_4.7H_2O$ for different p_{H2O} and 1°C/min heating rate

The trend of the reaction rate in Figure 38 is similar to the trend described by Topley and Smith in paragraph 2.2.2. Increasing the water vapor pressure from 8 mbar to 50 mbar results in a clear increase of the reaction rate for both dehydration reactions due to the formation of cracks and channels. Increasing the water vapor pressure further results again in a decrease of the reaction rate due to the increasing thermodynamic effects, as described in paragraph 2.2.2 . The Topley-Smith effect can also clearly be seen in the trend of the maximum values of the reaction rate, as shown in Figure 39. In this figure, the black- and red line represent the maximum values of the 7-6 dehydration and 6-1 dehydration respectively.

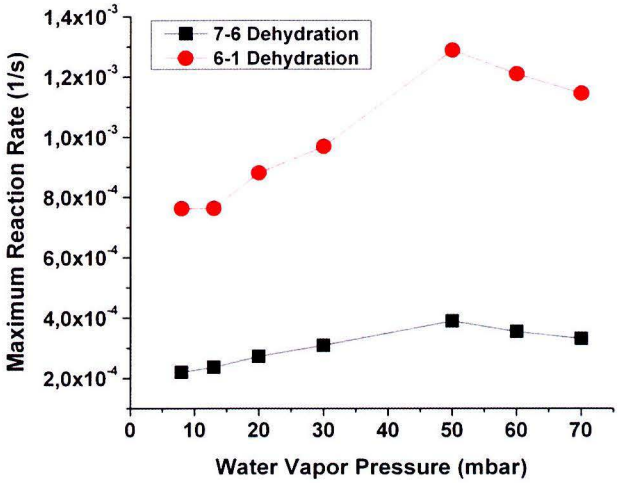

Figure 39: Maximum reaction rate for the dehydration of $MgSO_4.7H_2O$ for different p_{H2O} per mole H_2O

5.2.2 Kinetics parameters for the dehydration of $MgSO_4.7H_2O$

The FWO method described in chapter 3.2 is used to determine the activation energy (E_a) for the dehydration of $MgSO_4.7H_2O$. Hereto, the dehydration reactions were observed at different heating rates. Figure 40 shows the mass fraction reacted for the dehydration performed at 13 mbar p_{H2O} and at a heating rate of 1°C/min, 2°C/min and 5°C/min.

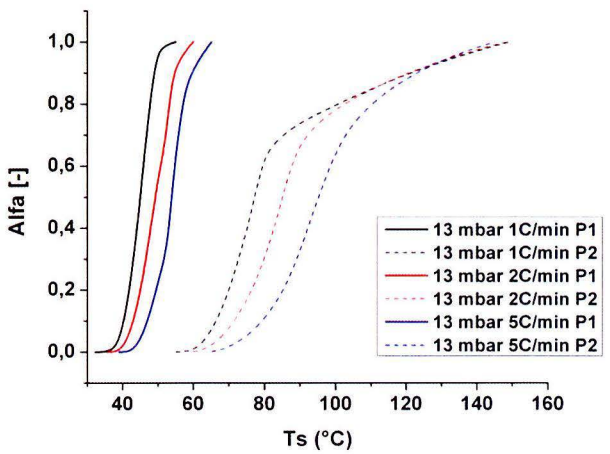

Figure 40: Mass fraction reacted for the dehydration of $MgSO_4.7H_2O$ at 13 mbar p_{H2O} and different heating rates

In Figure 40, the mass fraction reacted (α) is defined separately for the two dehydration reactions. The 7-6 dehydration is denoted as P1 (solid curve) and the 6-1 dehydration is denoted as P2 (dashed

curve). This makes it possible to analyze the two dehydration reactions separately and per mole H_2O reacted.

The onset temperature shifts for the different heating rates, as can be seen from Figure 40. This is a result of the finite reaction rate of dehydration. At increasing heating rates, the dehydration reaction is pushed away from its equilibrium, meaning that the kinetics of reaction cannot keep up with the heating rate.

For the FWO method, a consistent change in the onset temperature is necessary in order to determine the activation energy, as discussed in chapter 3.2. At the dehydration performed at 13 and 20 mbar p_{H2O} this consistent change in the onset temperature is present, but is absent for the dehydration performed at 30 mbar p_{H2O} and higher. The DSC system probably becomes more unstable at these higher water vapor pressures as a result of increased condensation in the system.

Due to this, it is only possible to determine the activation energy for the dehydration at 13 and 20 mbar p_{H2O}.

The activation energy corresponding to the dehydration at 13 and 20 mbar p_{H2O} is shown in the following figure:

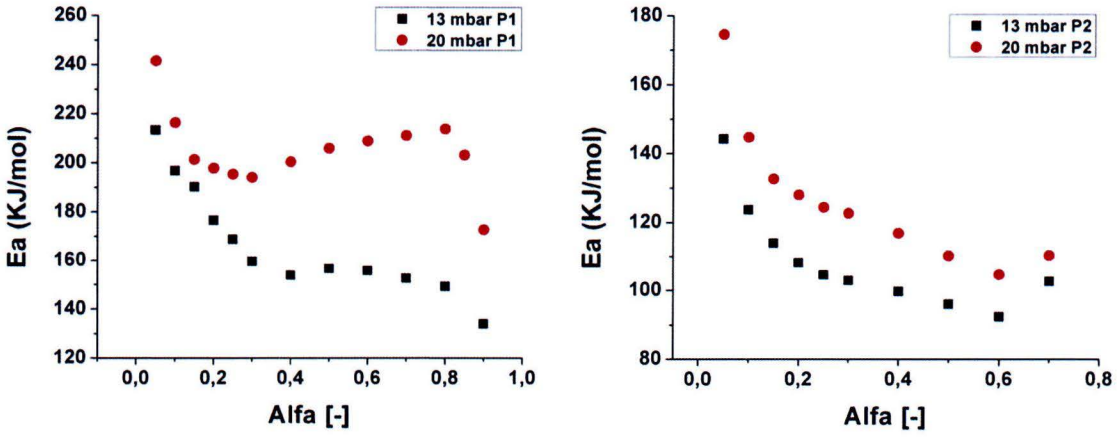

Figure 41: Activation energy for the 7-6 dehydration or P1 (left) and the 6-1 dehydration or P2(right) for different p_{H2O}

The activation energy for the dehydration of $MgSO_4.7H_2O$ is not constant, as can be seen from the figure above, which is a result of the complex character of the dehydration reaction. From Figure 41 it can also be seen that the E_a for the 7-6 dehydration is higher than the 6-1 dehydration, which is not conformal with findings presented in literature [7]. Ruiz et al. found that the activation energy increases for an increasing α, as shown in Figure 14. However, Ruiz et al. dehydrated the $MgSO_4.7H_2O$ in a nitrogen atmosphere, which changes the kinetics of reaction in comparison to dehydration in a wet atmosphere, as discussed in the previous paragraph.

In the initial phase of the dehydration process ($0,0 < \alpha < 0,3$ at P1) a sharp decrease is observed in the E_a. This may be related with the initial formation of cracks and channels which facilitate the water vapor removal in the sample. This might also explain the difference in E_a between the 7-6 dehydration and the 6-1 dehydration, for the formation of cracks and channels will probably take

place during the whole dehydration process, meaning that the water vapor removal is increasingly facilitated during the whole dehydration process.
A sharp drop in the E_a is also observed at the end of the 7-6 dehydration and the beginning of the 6-1 dehydration denoting the transition between the two dehydration reactions.
For the determination of E_a, it was assumed that the 6-1 dehydration was completed at 150°C. From Figure 35 can be seen however, that the 6-1 dehydration reaction is still ongoing at this temperature. This results in an increasing error in the measurements at $\alpha > 0,7$ at P2, rendering it impossible to accurately determine the activation energy for these mass fractions reacted.

Using the calculated values for the activation energy, the values for $A \cdot f(\alpha)$ can be calculated from the reaction rate according to the following equation, which is obtained by rewriting equation 10 and 11.

$$A \cdot f(\alpha) = \frac{d\alpha}{dt} \cdot \frac{1}{\exp\left(\frac{-E_a}{RT}\right)} \tag{22}$$

Using equation 22, the following values for $A \cdot f(\alpha)$ were found:

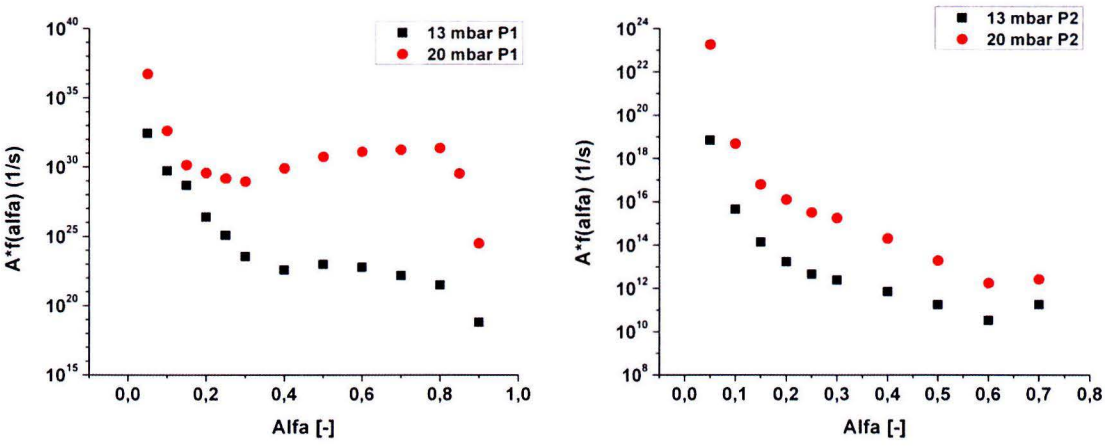

Figure 42: A.f(α) for the 7-6 dehydration or P1 (left) and the 6-1 dehydration or P2(right) for different p_{H2O}

Under the assumption that the empirically found values for *a* and *b* in table 2 are also valid for the dehydration of $MgSO_4.7H_2O$ at 13 and 20 mbar p_{H2O}, the pre-exponential factor can be determined from the activation energy. Based on these values for the pre-exponential factor, the following values for the reaction model equation can be determined:

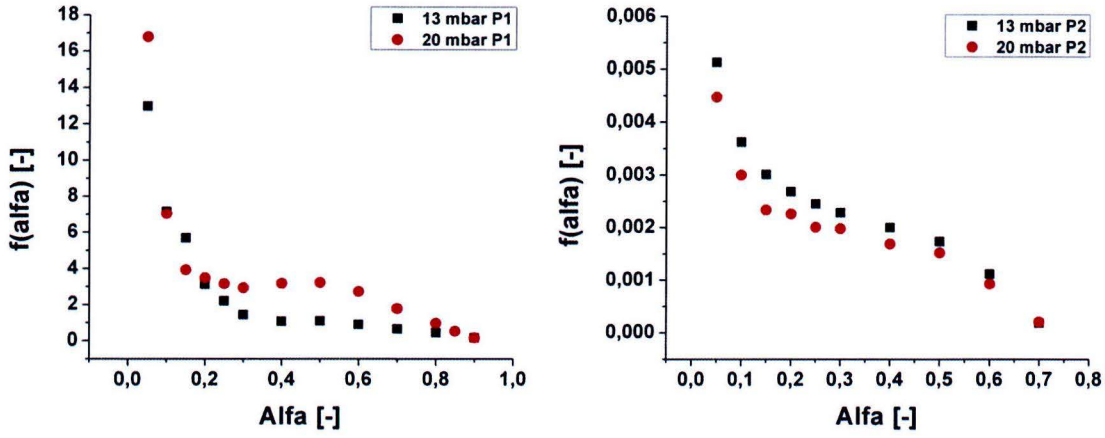

Figure 43: Reaction model equation for the 7-6 (left) and 6-1 (right) dehydration of $MgSO_4.7H_2O$ at 13 and 20 mbar p_{H2O}

The trend of the reaction model equation for the 7-6 dehydration is similar to the trend of the diffusion controlled reaction model equation, as shown in Figure 15. This implies that the diffusion rate of participants to or from an interface is of dominant influence on the rate of product formation. The diffusion of water through the $MgSO_4$ has thus the largest influence on the kinetics of reaction for this 7-6 dehydration.

The reaction model equation for the 6-1 dehydration is more complex and probably contains a combination of multiple reaction model equations. The decreasing trend suggests that the diffusion controlled reaction model equation is still of influence. In addition, the phase change from crystalline $MgSO_4.6H_2O$ to amorphous $MgSO_4.H_2O$ probably also has a large influence on the kinetic behavior of the material.

A more in-depth analysis of the reaction model equations or rate mechanisms is beyond the scope of this project.

5.2.3 Hydration of $MgSO_4$

Dehydration-rehydration cycle tests were performed using the HPDSC in order to investigate the hydration characteristics of $MgSO_4$. Hereto, the fully hydrated sample is first dehydrated to $MgSO_4.H_2O$ by heating the sample to 150°C at a heating rate of 1°C/min, as analyzed in paragraph 5.2.1. Next, the sample is cooled at a cooling rate of 1°C/min, which allows the sample to rehydrate again.

The cycle test performed at a water vapor pressure of 13 mbar and a heating/cooling rate of 1°C/min is shown in the following figure:

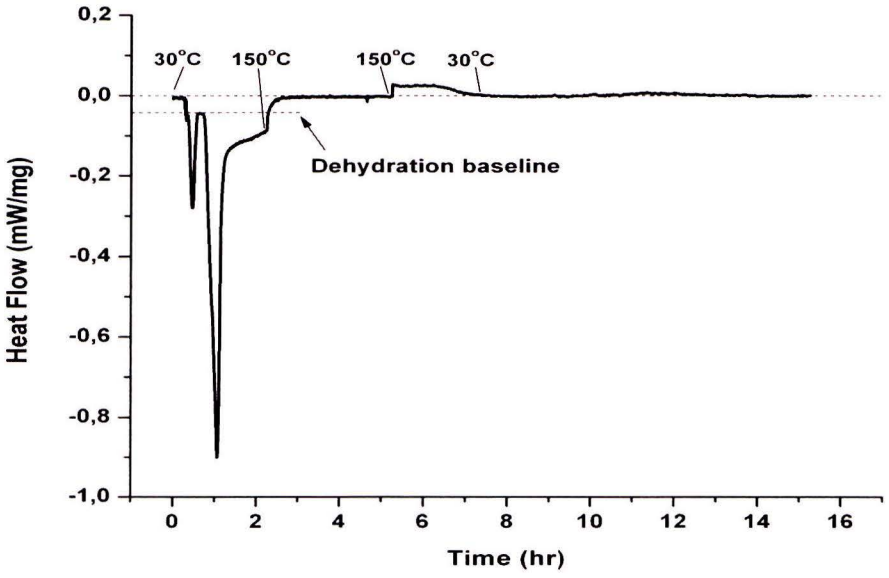

Figure 44: Dehydration-rehydration cycle of $MgSO_4$ at 13 mbar p_{H2O} and 1°C/min heating rate

For this cycle test, the sample was heated from 30°C to 150°C at a heating rate of 1°C/min, followed by an isothermal period of 3 hours. The sample was then cooled to 30°C again and was kept at this temperature for 8 hours, allowing the sample to rehydrate. Figure 44 shows no rehydration signal however. The exothermal signal which occurs after 5 hours is a shift in the baseline as a result of the change in the temperature program. At this time, the temperature program changes from an isothermal period to cooling of the sample. From Figure 44 can thus be concluded that rehydration at 13 mbar proceeds at too slow kinetics of reaction to allow visible observation using a DSC.
The amount of heat absorbed during dehydration can be calculated from the area under the DSC-signal, which is equal to -1074 kJ/kg. The theoretical amount of heat absorbed can be calculated using the values for the reaction enthalpy as presented in table 1 in chapter 3.1, giving a theoretical value of -1361 kJ/kg during dehydration of $MgSO_4.7H_2O$ to $MgSO_4.H_2O$. A possible explanation for this difference between the theoretical and measured amount of heat absorbed is the fact that the dehydration reaction to $MgSO_4.H_2O$ is not fully complete at 150°C, as can be seen from the trend in the above figure. In addition, an error can also be made by the manual definition of the baseline, which is required for the integration of the DSC-signal during dehydration. As can be seen from Figure 44, this baseline lies not at 0.0 mW/mg during dehydration, but at around 0.04 mW/mg.

In order to investigate the effect of the water vapor pressure on the kinetics of reaction during rehydration, a cycle test was performed at a water vapor pressure of 70 mbar, as shown in Figure 45.

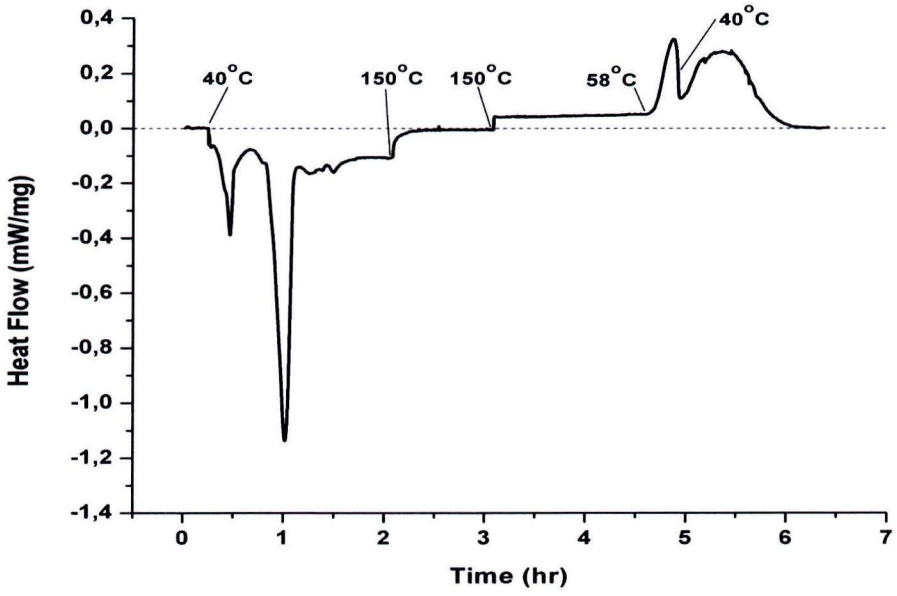

Figure 45: Dehydration-rehydration cycle of $MgSO_4$ at 70 mbar p_{H2O} and 1°C/min heating rate

For this cycle test, the sample was first heated from 40°C to 150°C, followed by an isothermal period of 1 hour. Then, the sample was cooled again to 40°C and was kept at this temperature for 90 minutes. A minimum temperature of 40°C was maintained to prevent overhydration, as discussed in paragraph 2.2.1. The temperature program used was shortened with respect to the temperature program used for the 13 mbar cycle test in order to prevent condensation as a result of this relative high water vapor pressure of 70 mbar.
Figure 45 shows a clear rehydration signal which starts when the sample is cooled to 58°C. This implies that the higher p_{H2O} increases the water vapor uptake during rehydration and thereby increases the kinetics of reaction. The shift in the baseline can also be observed after 3 hours of measurement and is consistent with the findings presented in Figure 44.
The heat release during hydration is equal to 697.3 kJ/kg, implying that about 65% of the heat absorbed during dehydration is released during hydration.

In order to analyze the effect of the dehydration water vapor pressure on the rehydration behaviour of the material, the p_{H2O} is set separately for the dehydration and rehydration reactions. Hereto, a cycle test was performed using a p_{H2O} of 13 mbar during dehydration and a p_{H2O} of 70 mbar during hydration. The results are shown in the following figure:

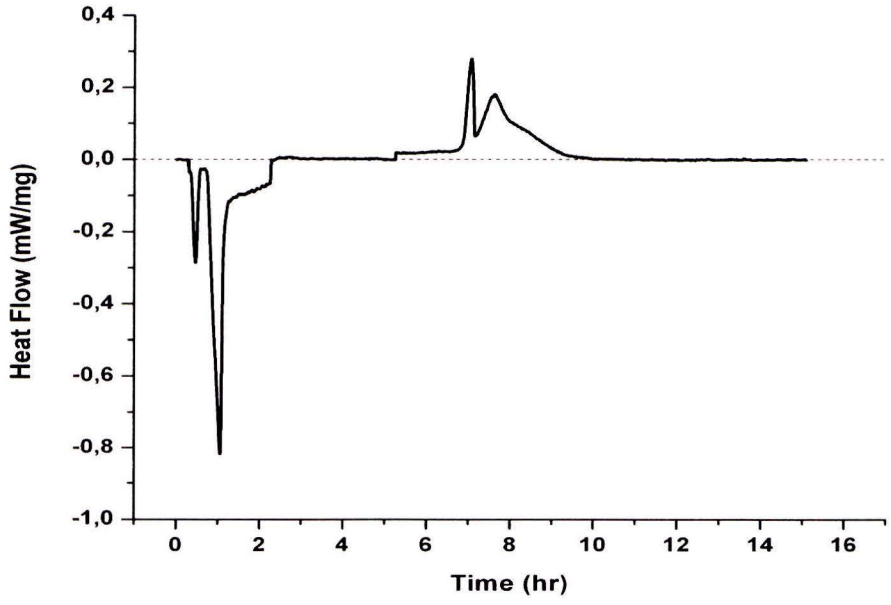

Figure 46: Dehydration-rehydration cycle test of $MgSO_4$ at 13/70 mbar (dehydration/rehydration) p_{H2O}

For this cycle test, the sample was heated from 30°C to 150°C with a heating rate of 1°C/min, followed by an isothermal period of 3 hours. Next, the sample was cooled to 40°C and kept at this temperature for 8 hours to allow rehydration of the sample. A minimum temperature of 40°C was again maintained during rehydration to avoid overhydration of the sample.
Figure 46 shows a similar rehydration signal as the cycle test performed at 70 mbar, indicating that the dehydration water vapor pressure doesn't influence the rehydration behaviour. This is conformal with the findings presented in Figure 35 and Figure 37 in paragraph 5.2.1, which show that the sample maintains its amorphous structure during dehydration at different water vapor pressures. The amount of heat released during hydration is equal to 686.8 kJ/kg, which is about equal to the heat release at the cycle test performed at 70 mbar, indicating again that the dehydration p_{H2O} is of no influence on the rehydration signal.

Figure 47 shows the DSC results for the rehydration of $MgSO_4$ at different water vapour pressures. These results were obtained using the same temperature program as for the 13/70 cycle test, as described above. The data for the dehydration is left out in this figure.
From Figure 47 it can be seen that the highest rehydration heat release was realised at 50 mbar p_{H2O}. These results are conformal with the findings presented in Figure 35 in paragraph 5.2.1, in which the highest rate of heat absorbed was also obtained at 50 mbar during dehydration. Thus, the highest kinetics of reaction are realised using a water vapor pressure of 50 mbar for both dehydration and rehydration.
The onset temperature shifts as a result of the different water vapor pressures. For rehydration, a higher water vapor pressure results in a lower equilibrium temperature and thus a lower onset temperature, as can be seen in Figure 47.

The figure shows two rehydration peaks per measurement. The first peak is represented by a solid line while the second peak is represented by a dashed line. Both rehydration peaks have a maximum at 50 mbar. These two peaks could be related to two rehydration reactions, each taking place at different temperatures. The first reaction takes place while the sample is being cooled to 40°C, while the second reaction takes place in the isothermal period of 40°C. At 30 mbar and lower, the second peak disappears, which could be related to the fact that the reaction at this p_{H2O} start during the isothermal period of 40°C, implying that the abovementioned temperature difference is now absent.

The heat release during hydration for these different cycle tests are shown in table 4. From this table it can be seen that the rehydration at 50 mbar results in a heat release of 775,5 kJ/kg. This is about 72% of the total amount of heat absorbed during dehydration (1074 kJ/kg). This 28% loss in efficiency could be partially related to the fact that the material is only rehydrated to $MgSO_4.6H_2O$. As described in paragraph 2.2.2, a water vapour pressure of at least 60 mbar is needed to rehydrate the salt hydrate further to $MgSO_4.7H_2O$. But as can be seen table 4, the rehydration heat release at 70 mbar is even less than the heat release at 50 mbar p_{H2O}, implying that an even higher water vapor pressure is required for complete rehydration.

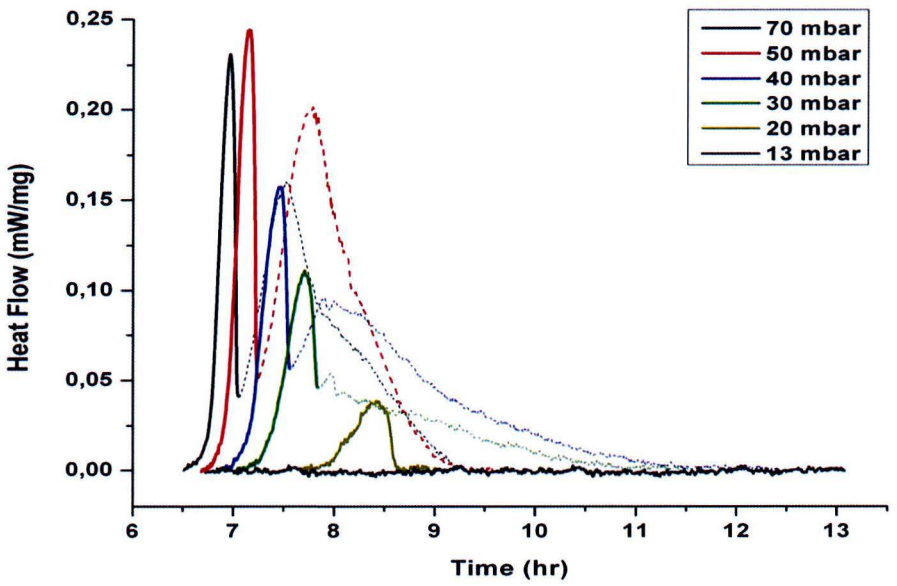

Figure 47: DSC signal for rehydration of $MgSO_4$ at different p_{H2O}

Hydration water vapor pressure (mbar)	Measured heat release during hydration (kJ/kg)
13	**0**
20	58.6
30	**369.8**
40	701.3
50	**775.5**
70	686.8

Table 4: Measured heat release during hydration at different hydration p_{H2O}

5.3 Application in Packed Bed Reactor

The Packed Bed Reactor is used to simulate the practical operating conditions in an open sorption heat storage system. The application of $MgCl_2.6H_2O$ will be discussed in paragraph 5.3.1 and the application of $MgSO_4.7H_2O$ in paragraph 5.3.2.

5.3.1 Application of $MgCl_2.6H_2O$

In the packed reactor, the air flow is driven through the sample, as discussed in chapter 4.3. During dehydration, a heating coil will heat the incoming air flow to 130°C at a massflow rate of 50L/min. The inlet water vapor pressure is equal to 13 mbar, both for the dehydration and hydration of $MgCl_2.6H_2O$. A dehydration temperature of 130°C is chosen in order to improve the dehydration rate with respect to dehydration at 110°C and to limit the decomposition rate with respect to dehydration at 150°C, as discussed in paragraph 5.1.1. The temperature in the bed is measured at different heights by means of thermocouples. The results of dehydration in the packed bed reactor are shown in the following figure:

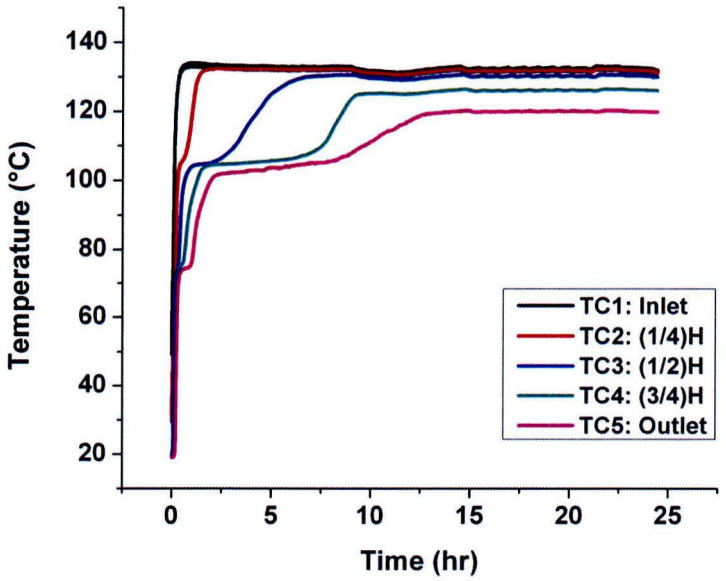

Figure 48: Dehydration of $MgCl_2.6H_2O$ in the packed bed reactor at 130°C , 13 mbar p_{H2O} and a massflow of 50L/min

From Figure 48 it can be seen that a steady state is achieved after about 13 hours. The outlet temperature is equal to 120°C at the given inlet temperature of 130°C. The UA value can be determined from these values as shown in equation 20, under the assumption that no further dehydration is taking place in this steady state. At these given reactor parameters, the UA value is equal to about 0.1 W/°C, implying that every °C of temperature difference between the reactor and the ambient results in a heat loss of 0.1 W.

After dehydration, the sample is hydrated again in order to analyze the heat release of the salt hydrate. A typical hydration temperature profile is shown in Figure 49.

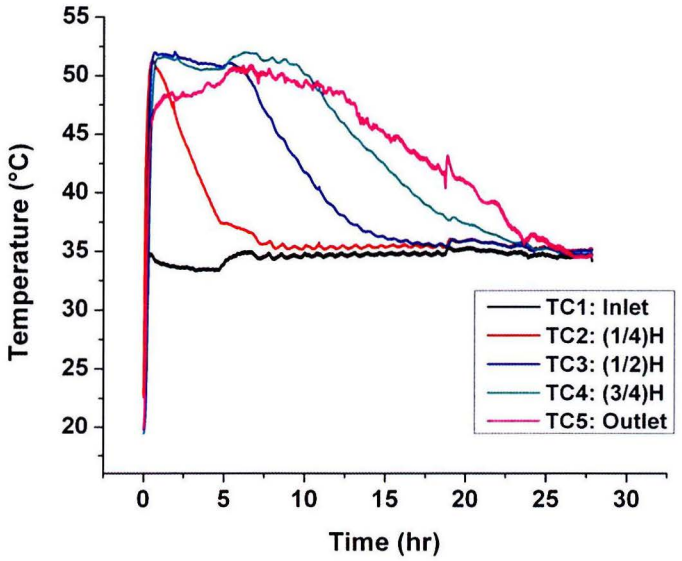

Figure 49: Hydration of $MgCl_2.6H_2O$ in the packed bed reactor at a T_{inlet} of 32°C, 13 mbar p_{H2O} and a massflow of 50L/min

During the hydration cycle as shown in the figure above, the reactor is exposed to moist air at 13 mbar at a massflow of 50L/min, with an inlet temperature equal to about 34°C. This inlet temperature is chosen in order to achieve a minimum temperature of 30°C in the bed, which is needed to prevent overhydration at a water vapor pressure of 13 mbar. Figure 49 clearly shows the heat release of the salt hydrate at different stages in the bed. A maximum temperature rise of about 16°C is achieved, heating the incoming air from 34°C to 50°C, as can be seen from the figure below. The PBR, with a volume of 0,65 dm^3, was able to deliver a temperature rise of 15 °C for about 10 hours.

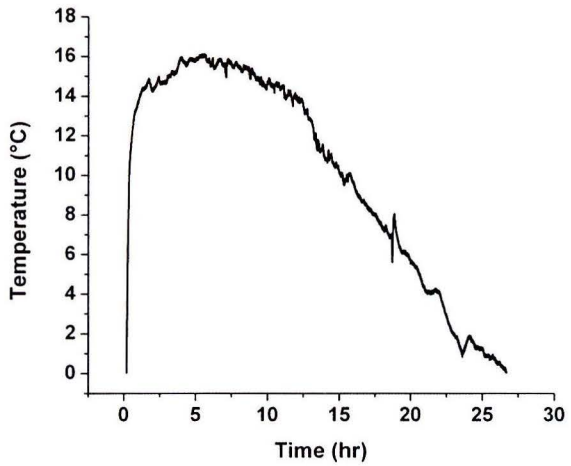

Figure 50: Temperature rise in the PBR for the hydration of $MgCl_2.6H_2O$ at a T_{inlet} of 34°C, 13 mbar p_{H2O} and a massflow of 50L/min

The heating power is calculated by the temperature difference between the incoming and outgoing air in the reactor, as described in equation 20. The results are shown in the Figure 51. From the area beneath the curve, the amount of heat released can be calculated. This hydration heat release is equal to 0.96 MJ. At a reactor volume of 0.65 dm^3, this corresponds to a heat release of 1.48 GJ/m^3. The density of the salt hydrate is equal to 1015 kg/m^3, based on a reactor volume of 0.65 dm^3 and a sample mass of 660 gram. The theoretical density of $MgCl_2.6H_2O$ is 1560 kg/m^3 [27], indicating that the porosity of the bed is equal to about 35%. The crystal energy density for the rehydration of $MgCl_2.2H_2O$ to $MgCl_2.6H_2O$ is equal to 1.93 GJ/m^3 [27], which gives in combination with the abovementioned porosity a maximum achievable heat release of 1.25 GJ/m^3. The difference between the maximum achievable heat release and the measured heat release can in the first place be explained by possible leakages in the system setup. For the calculation of the actual heat release it is assumed that a massflow of 50 L/min is driven through the reactor. It could be possible that leakages in the system setup reduce the actual massflow rate through the reactor, which thus results in a heat release lower than 1.48 GJ/m^3. In addition, it could also be possible that the sample is partially dehydrated to $MgCl_2.H_2O$ at a reactor temperature of 130°C. The rehydration of $MgCl_2.H_2O$ to $MgCl_2.6H_2O$ has a crystal energy density of 2.48 GJ/m^3, which is much higher than the prementioned 1.93 GJ/m^3 for the 2-6 rehydration.

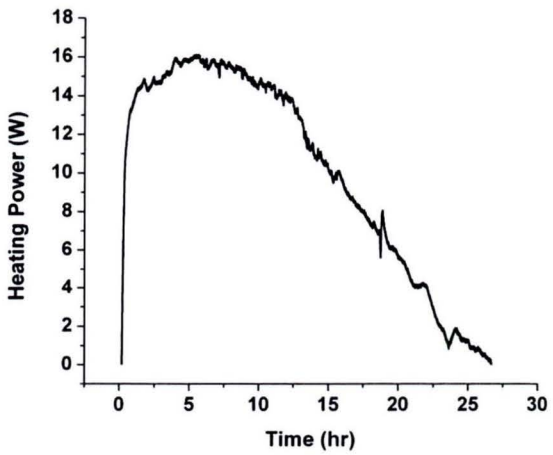

Figure 51: Hydration heating power of $MgCl_2.6H_2O$ at a T_{inlet} of 34°C, 13 mbar p_{H2O} and a massflow of 50L/min

In a practical seasonal heat storage system setup it is possible to heat the reactor inlet air by waste heat from the reactor outlet air, which will thus result in an increase of the reactor inlet temperature. In order to analyze this effect of the hydration heating power, the reactor inlet temperature is varied between 30°C and 50°C, as shown in Figure 52.

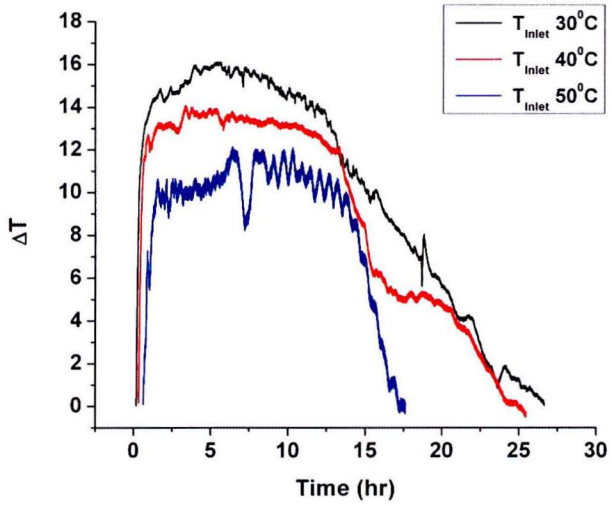

Figure 52: Temperature rise in the PBR for the hydration of $MgCl_2.6H_2O$ at varying T_{inlet}, 13 mbar p_{H2O} and a massflow of 50L/min

From the figure above it is made clear that an increase in the reactor inlet temperature results in a decrease in the temperature rise in the reactor. The absolute temperature in the reactor increases from 46°C to 61°C with an corresponding reactor inlet temperature increasing from 30°C to 50°C. The temperature difference with the ambient thus also increases, leading to an overall increase in the heat loss and thereby to an decrease in the temperature step.
The values for the heat loss at varying T_{inlet} are shown in table 5. Hereto, the average temperature in the reactor was determined based on the temperature measured by the three thermocouples in the bed.
Table 5 also shows that the heat release at a T_{inlet} of 50°C is much lower than at a T_{inlet} of 30°C and 40°C. This can be a result of the incomplete or slow rehydration at this higher reactor temperature. At a reactor temperature of 61°C, the 4-6 rehydration is in equilibrium, indicating that complete hydration is not possible at this temperature.

The massflow of the moist air is varied between 20 L/min and 50 L/min in order to analyze the effect of the massflow on the hydration heat release. The results of the corresponding temperature rise in the packed bed reactor are shown in Figure 53. The highest temperature rise is obtained at a massflow of 50L/min, and a subsequent decreasing trend can be observed with a decreasing massflow. As can be seen from equation 20, $\dot{q}_{in}$, $\dot{q}_{out}$ and $\dot{q}_{hydration}$ strongly depend on the massflow through the reactor whereas $\dot{q}_{loss}$ mainly depends on the temperature difference between the reactor and the ambient. This indicates that the heat losses become increasingly dominant with a decreasing massflow rate, resulting thus in a lower temperature rise in the reactor.
The hydration period increases with a decreasing massflow, as can clearly be seen from Figure 53, since the total amount of hydration-energy available in the bed remains the same.

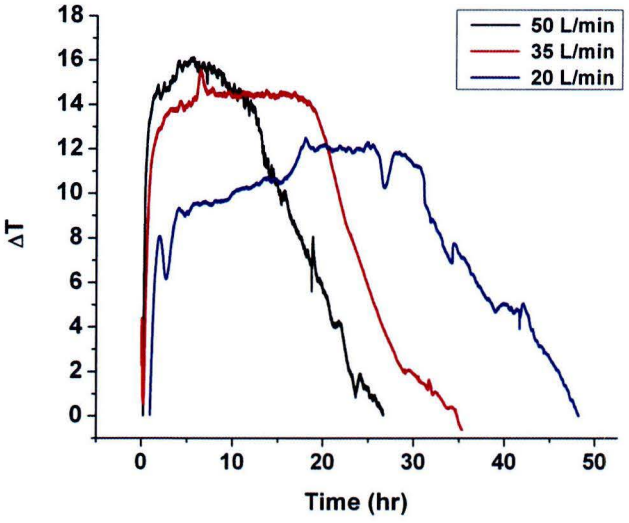

Figure 53: Temperature rise in the packed bed reactor for the hydration of $MgCl_2.6H_2O$ at a T_{Inlet} of 30°C, 13 mbar p_{H2O} and a varying massflow

The heating power corresponding to the temperature rise in Figure 53 is shown in Figure 54. The total heat release can be calculated by integration of this heating power. From table 5 can be seen that the heat release decreases with an decreasing massflow rate, which is again a result of the increasing effect of the heat losses, as discussed above.

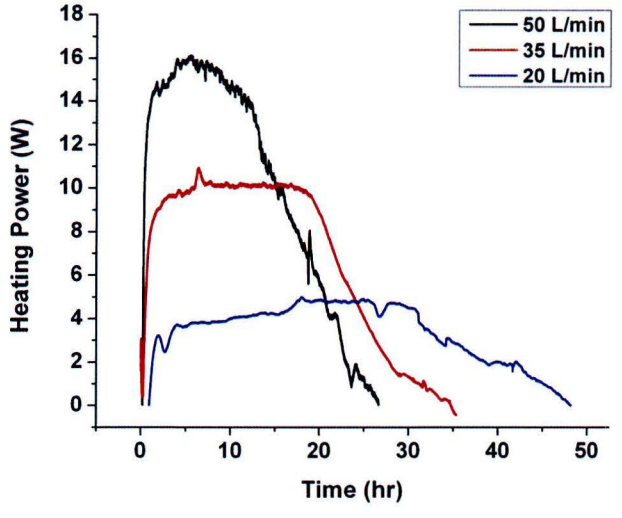

Figure 54: Hydration heating power of $MgCl_2.6H_2O$ at a T_{Inlet} of 30°C, 13 mbar p_{H2O} and a varying massflow

T_{Inlet} (°C)	Massflow rate (L/min)	Heat loss (MJ)	Heat release (MJ)	Heat release (GJ/m^3)
30	50	0.204	0.96	1.48
40	50	0.226	0.81	1.25
50	50	0.243	0.54	0.83
30	20	0.398	0.58	0.89
30	35	0.272	0.86	1.32
30	50	0.204	0.96	1.48

Table 5: Properties of hydration of $MgCl_2.2H_2O$ in the packed bed reactor

5.3.2 Application of $MgSO_4.7H_2O$

For the dehydration of $MgSO_4.7H_2O$ in the packed bed reactor, the reactor was heated to 150°C with a massflow rate of 50 L/min and a water vapor pressure of 13 mbar. The results of dehydration are shown in the following figure:

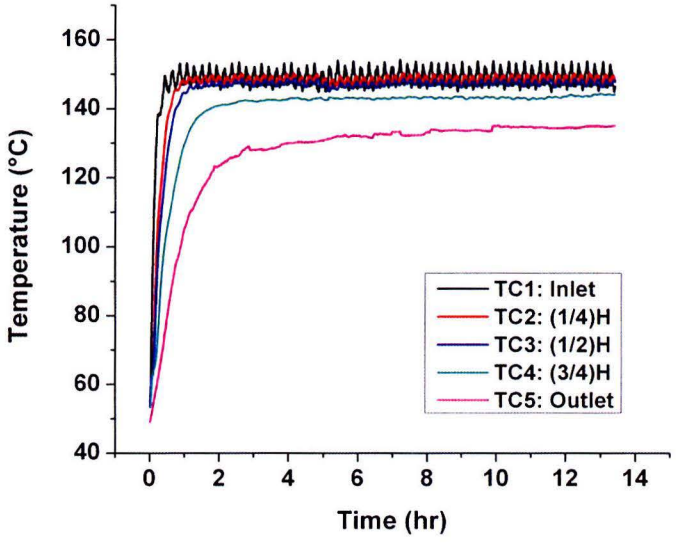

Figure 55: Dehydration of $MgSO_4.7H_2O$ in the packed bed reactor at a T_{Inlet} of 150°C, 13 mbar p_{H2O} and a massflow of 50L/min

The UA-value can again be determined from the dehydration signal. This value is equal to about 0.1 W/°C, which is consistent with the UA-value determined from the dehydration signal of $MgCl_2.6H_2O$. After dehydration, the sample is cooled again in order to allow rehydration of the bed. The hydration performed at a massflow rate of 50 L/min, T_{Inlet} of 30°C and p_{H2O} of 13 mbar is shown in Figure 56.

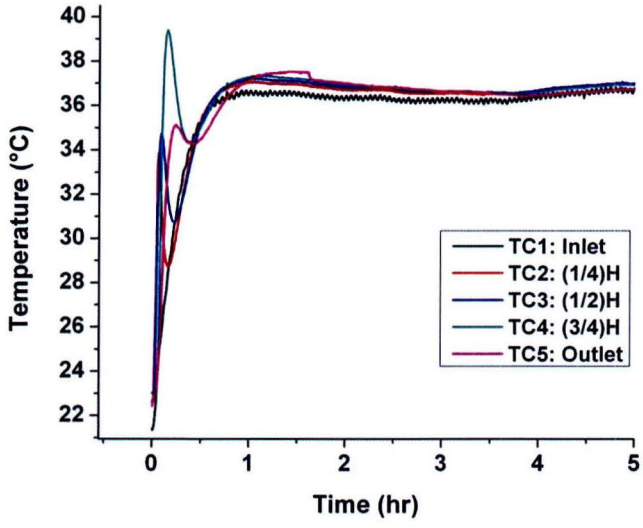

Figure 56: Hydration of $MgSO_4.7H_2O$ in the packed bed reactor at a T_{Inlet} of 35°C, 13 mbar p_{H2O} and a massflow of 50L/min

Two peaks can be distinguished from the hydration signal shown in the figure above, which is consistent with the findings presented in paragraph 5.2.3. These two peaks can be related to two different hydration reactions, as described before. From Figure 56 it can also be seen that only a minor temperature step is realized at a water vapor pressure of 13 mbar, which can be related to the slow water vapor uptake of the salt hydrate. In the first half hour of hydration, the temperature in the bed increases with an increasing bed height. This indicates that not all water vapor is taken up by the salt in the lower stages in the bed, which can again be attributed to the slow hydration kinetics.

In order to increase the hydration kinetics, the water vapor pressure during hydration is increased. Figure 57 shows the hydration signal at a water vapor pressure of 50 mbar and a T_{Inlet} of 50°C. At this water vapor pressure, a minimum temperature of 50°C is required to prevent condensation in the experimental setup.

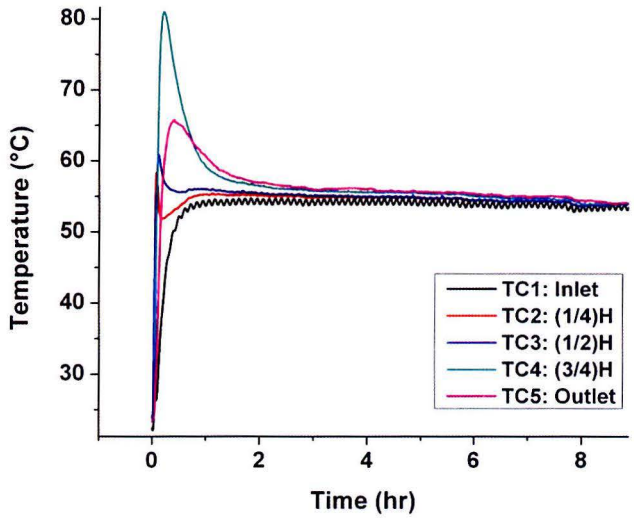

Figure 57: Hydration of $MgSO_4.7H_2O$ in the packed bed reactor at a T_{Inlet} of 50°C, 50 mbar p_{H2O} and a massflow of 50L/min

Figure 57 and Figure 58 clearly show that the hydration temperature step increases with an increasing water vapor pressure. A maximum temperature step of 18°C was realized at 50 mbar p_{H2O}, as can be seen from Figure 58, whereas at 13 mbar p_{H2O}, a maximum temperature step of 5°C was realized. This can be explained by the increase in the amount of water vapor present in the air flow. According to equation 21, the water vapor content in the air flow at 50 mbar p_{H2O} is about four times higher than at 13 mbar p_{H2O}, resulting thus in a higher $\dot{q}_{hydration}$. The period in which a temperature step is realized also increases with an increasing water vapor pressure. At 50 mbar p_{H2O}, the heating power is sufficient to effectively heat the outgoing air for about 10 hours, as can be seen from Figure 58. At 13 mbar p_{H2O} the heat losses in the bed are too high with respect to the heating power, resulting thus in a short effective heating period of 4 hours.

The hydration properties of $MgSO_4H_2O$ are shown in table 6. From this table it can be seen that the amount of heat released is about 11 times as high at 50 mbar p_{H2O} in comparison to 13 mbar p_{H2O}, while the heat losses are only twice as high as a result of the increased T_{Inlet}. Increasing the water vapor pressure during hydration thus reduces the relative heat losses. The reactor inlet temperature is set to 50°C in order to prevent condensation at 50 mbar p_{H2O}. At this water vapor pressure, a heat release of 0.148 GJ/m^3 is realized, which is much lower than the heat release of 0.83 GJ/m^3 for the hydration of $MgCl_2.2H_2O$ at a T_{Inlet} of 50°C.

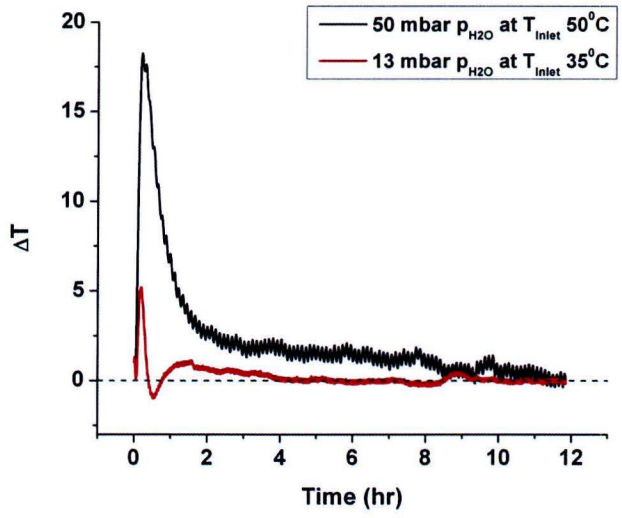

Figure 58: Temperature rise in the packed bed reactor for the hydration of $MgSO_4.H_2O$ at 13 and 50 mbar p_{H2O} and a massflow rate of 50L/min

Reactor inlet temperature (°C)	**Massflow rate (L/min)**	Water vapor pressure (mbar)	Heat loss (MJ)	Heat release (kJ)	Heat release (GJ/m^3)
30	**50**	**13**	**0.3**	**8.44**	**0.013**
50	50	50	0.73	96.5	0.148

Table 6: Properties of hydration of $MgSO_4.7H_2O$ in the packed bed reactor

6 Conclusions

The hydrolysis of $MgCl_2.6H_2O$ was investigated using a tubular furnace in combination with a water bath and additional pH sensor. It was found that hydrolysis occurs in the whole dehydration range of $MgCl_2.6H_2O$ to $MgCl_2.H_2O$, with the highest hydrolysis rates after dehydration to $MgCl_2.2H_2O$. The mass decomposition as a result of the hydrolysis at a reactor temperature of 110°C was limited at around 4% after a period of 350 hours. At this furnace temperature, the dehydration of $MgCl_2.6H_2O$ was limited to $MgCl_2.2H_2O$ after a dehydration period of also 350 hours, which suggests that the dehydration and hydrolysis occur mainly simultaneous. At 150°C however, complete hydrolysis was realized after about 500 hours in the tubular furnace. At this higher furnace temperature, further dehydration to $MgCl_2.H_2O$ was possible, allowing also further hydrolysis of the sample. A minimum mass decomposition of 1.2% per dehydration-hydration cycle in de dehydration range of $MgCl_2.6H_2O$ to $MgCl_2.2H_2O$ is possible at a dehydration temperature of 150°C. Hereto it is required that the system setup is well regulated with respect to temperature distributions within the reactor in combination with accurate observations of the dehydration state.
Changing the sample mass and thereby the sample thickness resulted in a change in the dehydration and hydrolysis rate. The vapor pressure in the sample decreases with a decreasing sample thickness resulting in a subsequent increase of the dehydration and hydrolysis rate. The increase in both rates compensate each other in the dehydration range of $MgCl_2.6H_2O$ to $MgCl_2.2H_2O$, resulting in an identical mass decomposition after dehydration to $MgCl_2.2H_2O$. This same effect was found for a varying massflow rate.

A high pressure DSC was used to investigate the kinetics of reaction for the dehydration of $MgSO_4.7H_2O$. It was found that the kinetics of reaction can be increased with an increasing water vapor pressure, consistent with the Topley-Smith effect. The lowest reaction rate was found at a p_{H2O} of 8 mbar while the highest reaction rate was achieved at 50 mbar p_{H2O}.
Several dehydration-hydration cycling tests were performed in the HPDSC at different p_{H2O}. It was found that the increase of the kinetics of reaction during dehydration had no effect on the subsequent hydration kinetics of the salt hydrate. An increase in the water vapor pressure during hydration resulted in an increase of the hydration kinetics up to a maximum at 50 mbar p_{H2O}. The maximum observed heat release during hydration was equal to about 72% of the heat absorbed during dehydration. However, hydration at 50 mbar p_{H2O} requires a water source of 35°C in order to generate this required water vapor pressure, thereby limiting the overall efficiency of the sorption heat storage system.

Finally, both salt hydrates were used for dehydration-hydration cycles in a packed bed reactor, which simulates the practical operating conditions of an open sorption heat storage system.
The PBR, with a volume of 0.65 dm^3, was able to deliver a temperature rise of 15 °C for about 10 hours at a corresponding heating power of 15W during the hydration of $MgCl_2.2H_2O$. A heat release of 1.48 GJ/m^3 was achieved at a reactor inlet temperature of 30°C, 13 mbar p_{H2O} and a massflow rate of 50 L/min. The hydration of $MgSO_4.H_2O$ resulted in a temperature rise of 5°C and 18°C for about 30 minutes at a water vapor pressure of 13 and 50 mbar respectively. A corresponding heat release of of 0.013 GJ/m^3 and 0.148 GJ/m^3 was realized, indicating that $MgCl_2.6H_2O$ is much better suited for the application as a heat storage material.

References

[1] H.A. Zondag, R. Schuitema, L.P.J. Bleijendaal, J. Cot Gores, V.M. van Essen, W.G.J. Van Helden and M. Bakker, *R&D of thermochemical reactor concepts to enable seasonal heat storage of solar energy in residential houses*, Proceedings of the ASME 2009 3rd International Conference of Energy Sustainability, San Fransisco (2009)

[2] W. Eichhammer and D. Bosseboeuf, *Energy Efficiency Trends and Policies in the Industrial Sector in the EU-27, Lessons from the ODYSSEE/MURE project*, ADEME Editions, Paris (2009)

[3] K. Visscher, J.B.J. Veldhuis, H.A.J. Oonk, P.J. van Ekeren, and J.G. Blok, *Compacte chemische seizoenopslag van* zonnewarmte, ECN Report ECN-C-04-074 (2004)

[4] H.A. Zondag, B.W.J. Kikkert, S. Smeding and M. Bakker, *Thermochemical seasonal solar heat storage with $MgCl_2.6H_2O$: First up scaling of the reactor*, Proceedings of the International Conference for Sustainable Energy Storage, Belfast (2011)

[5] C.J Ferchaud, H.A. Zondag, A. Rubino and R. de Boer, *Seasonal sorption heat storage – Research on thermochemical materials and storage performance*, Proceedings of the Heat Powered Cycles Conference 2012, Alkmaar (2012)

[6] V.M. van Essen, L.P.J Bleijendaal, B.W.J. Kikkert, H.A. Zondag, M. Bakker and P.W. Bach, *Development of a compact heat storage system based on salt hydrates*, proceeding international conference on solar heat, cooling and buildings IEA, Eurosun 2010 (2010)

[7] V.M. van Essen, J. Cot Gores, L.P.J. Bleijendaal, H.A. Zondag, R. Schuitema and W.G.J. van Helden, *Characterization of salt hydrates for compact seasonal thermochemical storage*, Proceedings of the ASME 2009 3rd International Conference on Energy Sustainability, San Fransisco (2009)

[8] H.A. Zondag, V.M. van Essen, L.P.J. Bleijendaal, B.W.J. Kikkert and M. Bakker, *Application of $MgCl_2.6H_2O$ for thermochemical seasonal solar heat storage*, Proceedings IRES 2010 conference, Berlin (2010)

[9] V. M. van Essen, H. A. Zondag, J. Cot Gores, L. P. J. Bleijendaal, M. Bakker, R. Schuitema, W. G. J. van Helden, Z. He and C. C. M., Rindt *Characterization of $MgSO_4$ Hydrate for Thermochemical Seasonal Heat Storage*, Journal of Solar Energy Engineering 131(4), 041014 (2009)

[10] I.M. van de Voort, *Characterization of thermal storage material*, ECN Master thesis report (2007)

[11] G. J. Kipouros and D.*R.* Sadoway, *A thermochemical analysis of the production of anhydrous $MgCl_2$*, Journal of Light Metals (2001)

[12] C.J Ferchaud, H.A. Zondag, J.B.J. Veldhuis and R. de Boer, *Study of the reversible water vapour sorption process of $MgSO_4.7H_2O$ and $MgCl_2.6H_2O$ under the conditions of seasonal solar heat storage,* Proceedings of the 6th European Thermal Sciences Conference, Eurotherm 2012, (2012)

[13] S. Siegesmund and R. Snelthlage, *Stone in Architecture - Properties, durability, 4th Editions,* Springer, 277-281 (2011)

[14] G. Watelle-Marion, M. Lallemant and G. Bertrand, *Abnormal Phenomena observed when an hydrated salt-water vapour system is abruptly placed far from its conditions of equilibrium,* Reactivity of solids, proceeding of the 7th inter. Conf.,722-732 (1972)

[15] S. J. Chipera, D. T. Vaniman, *Experimental stability of magnesium sulfate hydrates that may be present on Mars,* Geochemica et Cosmochemica Acta (2006)

[16] B. Topley and M. L. Smith, *Kinetics of salt-hydrate dissociations:* $MnC_2O_4,2H_2O = MnC_2O_4 + 2H_2O$, Journal of Chemical Society, 321–325 (1935)

[17] A.M. Kaushal, V.R. Vangala and R. Suryanarayanan, *Unusual effect of water vapor pressure on dehydration of dibasic calcium phosphate dehydrate,* Journal of Pharmaceutical Sciences 100, 1456-1466, (2010)

[18] M. Lallemant and G. Watelle-Marion, *Dégradation thermique du sulfate de magnésium heptahydrate sous pression de vapeur d'eau contrôlée. Mécanisme observé de 10-1 a 40 Torr,* C.R. Acad. Sc. Paris, t. 264 (1967)

[19] R. W. Ford and R.W. Frost, *The low pressure dehydration of magnesium sulphate heptahydrate and cobaltous chloride hexahydrate,* Canad. J. Chem. 34, 591 (1956)

[20] H.H. Emons, G. Ziegenbalg, R. Naumann and F. Paulik, *Thermal decomposition of the magnesium sulfate hydrates under quasi-isothermal and quasi-isobaric conditions,* Journal of Thermal Analysis 36, 1265-1279 (1990)

[21] H.A. Zondag, *Thermal Energy Storage,* (2011), page 187

[22] E. Ruiz-Agudo, J.D. Martin-Ramos, C. Rodriguez-Navarro, *Mechanism and Kinetics of Dehydration of Epsomite Crystals Formed in the Presence of Organic Additives,* J. Phys. Chem B 111, 41-52, (2007)

[23] A.K. Galwey and M.E. Brown *Thermal decomposition of ionic solids,* Elsevier, Amsterdam (1999), page 184

[24] A.K. Galwey and M.E. Brown *Thermal decomposition of ionic solids,* Elsevier, Amsterdam (1999), page 152

[25] A.K. Galwey and M.E. Brown *Thermal decomposition of ionic solids,* Elsevier, Amsterdam (1999), page 169

[26] A.K. Galwey and M.E. Brown *Thermal decomposition of ionic solids,* Elsevier, Amsterdam (1999), page 149

[27] H.A. Zondag, *Thermal Energy Storage,* (2011), page 193

Appendix

A1 Measurement Techniques

A.1.1 Thermogravimetry

Thermogravimetry (TG) is used to measure the mass change of a certain sample. This measurement technique can be used to determine the release or uptake of water during dehydration or rehydration of a salt hydrate. The change in mass is measured by a microbalance which is enclosed by a furnace. The furnace can be heated or cooled by a predefined temperature program. Non-isothermal measurements provide information about the temperature range in which a certain reaction or phase transition occurs. The mass change for every reaction can be determined by means of the trend in the TG signal. With TG it is also possible to analyze the kinetics of reaction by determination of the reaction rate, $\frac{d\alpha}{dt}$, in which α is the mass fraction reacted.
The water vapor pressure inside the furnace can also be controlled, which makes it possible to simulate the practical conditions of seasonal heat storage.

A.1.2 Differential Scanning Calorimetry

Differential Scanning Calorimetry (DSC) is used to determine the rate of heat absorbed or released during a physical transformation of a certain material. When a sample undergoes a physical transformation such as a phase transition, heat can be released (exothermic reaction) of absorbed (endothermic reaction). By observing the difference in heat flow between a material sample and a reference sample, DSC is able to measure the amount of heat required or released during such a transition.
The DSC signal contains information about the heat rate as a function of time and temperature, which enables the determination of the onset temperature and transition temperature of individual reactions, such as the dehydration and hydration reactions of salt hydrates. The mass fraction reacted, α, can be determined by the area under the DSC signal, which also enables the determination of the reaction rate, $\frac{d\alpha}{dt}$. This makes DSC a powerful tool to analyze the kinetics of reaction.

A.1.3 X-ray Diffraction

X-ray diffraction (XRD) is used to determine the crystalline structure of a certain material. XRD uses CuK_α X-ray radiation in order to obtain a diffraction pattern, which consists of the diffraction intensity as a function of the diffraction angle. The angle at which a peak occurs in the diffraction pattern gives information about the preferred crystallographic orientation. These peaks in the diffraction pattern are the result of constructive interference from successive lattice planes in the crystal structure, described by Bragg's law:

$$2d \cdot sin\theta = n\lambda \quad \text{(A1)}$$

Where d is the interplanar distance, θ is half of the diffraction angle, n is an integer that represents the order of the diffraction peak and λ is the wavelength of the X-rays. The difference in the pathway between beams diffracted from consecutive planes is equal to $2d \cdot sin\theta$, as can be seen from Figure 59. When these diffracted beams are in phase, the signal increases due to constructive interference. The position of the diffraction peak therefore gives information about the structural arrangement of the atoms in the material.

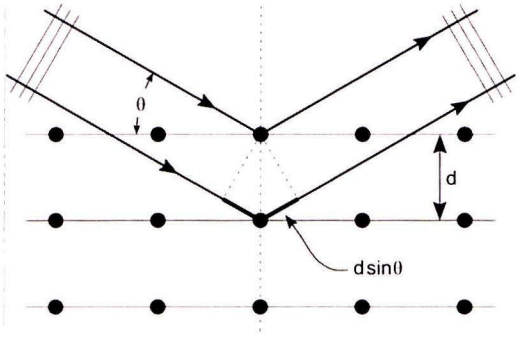

Figure 59: Schematic representation of Bragg's law

A.1.4 Scanning Electron Microscope and Energy Dispersive Analysis of X-rays

The composition of partially dehydrated $MgCl_2.6H_2O$ was determined using a Scanning Electron Microscope (SEM) in combination with the Energy Dispersive Analysis of X-rays (EDAX). The SEM uses a beam of accelerated electrons to scan the surface of the sample in vacuum. The accelerated electrons interact with the atoms of the sample, which results in the emission of secondary electrons and electromagnetic radiation. This emission of secondary electrons and electromagnetic radiation produces a signal which contains information about the surface topography and the composition of the sample.

A.1.5 pH-measurements

pH-measurements are used to determine the amount of hydrogen ions absorbed by a water bath. Pure water at a temperature of 25°C has a pH equal to 7. Solutions with a pH less than 7 are acidic whereas solutions with a pH larger than 7 are basic or alkaline. The pH of a water bath is measured using a Mettler-Toledo Inlab Expert Pro pH-sensor. The pH can be calculated in the following way:

$$pH = -log[H^+] \quad \text{(A2)}$$

With $[H^+]$ being the concentration of hydrogen ions in mole/liter.
The concentration of H^+ of a water bath can be calculated by rewriting equation 17:

$$[H^+] = 10^{-pH} \quad \text{(A3)}$$

A2 Temperature profile of the tubular furnace

The figure below shows the temperature profile of the tubular furnace set at 130°C. The tubular furnace is 53 cm long and the crucible in which the salt hydrate is placed is 12 cm long. The dashed red lines represent the boundaries between which the crucible is placed. The resulting temperature in the salt hydrate bed varies between 132,1°C and 129,5°C.

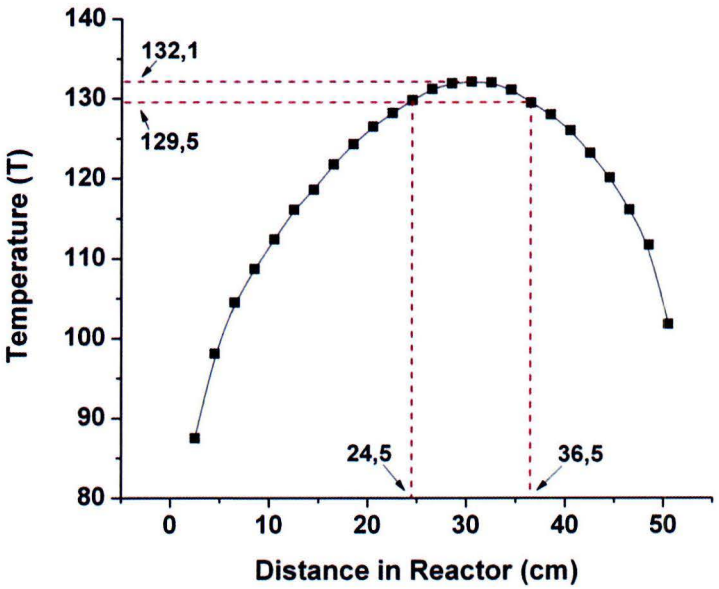

Figure A2-1: Temperature profile of the tubular furnace set at 130°C